

Irradiation hardening and ductility loss of Eurofer97 steel variants after neutron irradiation to ITER-TBM relevant conditions

Arunodaya Bhattacharya^{a*}, Xiang Chen^a, Tim Graening^a, Josina W. Geringer^a, Jordan Reed^a, Jean Henry^c, Luciano Pilloni^d, Dmitry Terentyev^e, Athina Puype^f, Thak Sang Byun^a, Yutai Katoh^a, Michael Rieth^b, Steven J. Zinkle^{a,g}

^a Materials Science and Technology Division, Oak Ridge National Laboratory, 1 Bethel Valley Road, Oak Ridge, 37831, TN, USA.

^b Karlsruhe Institute of Technology, IAM-AWP, Hermann-von-Helmholtz-Platz 1, 76344 Eggenstein-Leopoldshafen, Germany

^c CEA, DEN, Service de Recherches Métallurgiques Appliquées, Laboratoire d'Analyse Microstructurale des Matériaux, Université Paris-Saclay, 91191, Gif-sur-Yvette, France.

^d ENEA CR-Casaccia, Via Anguillarese 301 S.P. 059, 00123 Santa Maria di Galeria, Rome, Italy.

^e Belgian Nuclear Research Centre, SCK•CEN, Mol, 2400, Belgium.

^f OCAS NV, Pres. J.F. Kennedylaan 3, 9060 Zelzate, Belgium.

^g University of Tennessee, Knoxville, 37996, TN, USA.

*Corresponding author:

Postal Address: Materials science and technology division, ORNL, 1 Bethel valley road, 37831, USA.

Email: bhattacharya@ornl.gov

Tel: +18655741296

Co-author email addresses in order of appearance:

chenx2@ornl.gov

graeningt@ornl.gov

geringerjw@ornl.gov

reedjd@ornl.gov

jean.henry@cea.fr

luciano.pilloni@enea.it

dmitry.terentyev@sckcen.be

athina.puype@ocas.technology

byunts@ornl.gov

szinkle@utk.edu

katohy@ornl.gov

michael.rieth@kit.edu

Note: This manuscript has been authored by UT-Battelle, LLC under Contract No. DE-AC05-00OR22725 with the U.S. Department of Energy. The United States Government retains and the publisher, by accepting the article for publication, acknowledges that the United States Government retains a non-exclusive, paid-up, irrevocable, worldwide license to publish or reproduce the published form of this manuscript, or allow others to do so, for United States Government purposes. The Department of Energy will provide public access to these results of federally sponsored research in accordance with the DOE Public Access Plan (<http://energy.gov/downloads/doe-public-access-plan>).

Abstract

Ten Eurofer97 steel variants, produced by non-standard fabrication-processing routes and modified alloying chemistries, were studied by neutron irradiations in the high flux isotope reactor. The irradiations were performed to ITER-TBM relevant conditions of $\sim 255\text{-}350\text{ }^{\circ}\text{C}$, 2.94 - 3.24 dpa. We quantified the irradiation-induced degradation of the steels using mechanical property tests. All the steels suffered from irradiation hardening, where a significant increase in Vickers microhardness and yield stress (σ_{YS}) occurred, accompanied with severe loss of tensile elongation. The extent of hardening was material dependent. For $T_{irr} = 300 \pm 30\text{ }^{\circ}\text{C}$, most steels showed σ_{YS} increase in the range of $\sim 30\%$ to as high as $\sim 66\%$, except for a low temperature tempered steel with σ_{YS} increase below 15%. Despite large losses in elongation, most failures were ductile. Significant post-necking ductility was retained with reduction in area (RA) between 65-75%, but $< 50\%$ for low temperature tempered steels. The ultimate tensile stress to yield stress (σ_{UTS}/σ_{YS}) ratios decreased significantly after irradiation, highlighting irradiation-induced strain hardening capacity reduction. No major effect of irradiation on the plastic instability stress (σ_{PIS}) and true fracture stress of the steels was observed. By comparing the tensile stresses in true stress units and with literature, the results suggest that RAFM steel designing should target materials with a large separation between σ_{PIS} and σ_{YS} , to ensure the materials can maintain large work hardening and uniform deformation capability after irradiation. The tensile data of the steels additionally revealed a compelling evidence of an inverse trend between the change in RA and increase in σ_{YS} of the neutron irradiated Eurofer97 type steels.

Keywords: Eurofer97 steel; neutron irradiation; tensile properties, irradiation-hardening, fracture; reduction in area

1. Introduction

The structural materials for the first wall/blanket (FW/B) and plasma-facing components inside a power generating fusion reactor will be exposed to high thermo-mechanical and neutron loads [1–3]. The radiation damage caused by the neutrons combined with simultaneous generation of harmful transmutation products like hydrogen and helium at elevated operating temperatures will severely degrade the steel properties [4–6]. Owing to several advantageous characteristics such as high thermal conductivity, low thermal expansion coefficient and resistance to cavity swelling as compared to the austenitic steels, the ~9% Cr reduced activation ferritic martensitic (RAFM) steels are the most promising FW/B material candidates [2,7–9]. Typically manufactured in a normalized/tempered state with restrictions on activation prone elements (Nb, Mo, Co, Ni, Al etc.), RAFM steels consist of a tempered martensitic lath structure decorated with coarse $M_{23}C_6$ ($M = Fe, Cr, W$) carbides on lath-, packet- and prior-austenite grain boundaries (PAGBs), and smaller, ~30-40 nm diameter, MX ($M = Ta, V, X = C, N$) carbo-nitrides located mostly inside the laths [8,10]. Among the various RAFM steels being researched globally, Eurofer97 steel is the European reference material for the FW/B of the DEMO reactor produced after normalization at ~980 °C/30 min and tempering at ~750-760 °C/90 min [11,12].

Eurofer97 steel has been extensively researched using numerous irradiation tools such as neutron irradiations in materials test reactors, spallation neutron sources and heavy ion irradiations [9,13–23]. These results have highlighted the differing irradiation damage microstructure phenomenon including the formation of dislocation loops [19,23,24], cavities/bubbles [9,14,20], radiation-induced segregation (RIS) of solutes to grain boundaries/dislocation loops [25], and radiation induced/enhanced precipitation (RIP/REP) of solutes complexes such as Cr, Mn, Ni and Si [22,25]. A consequence of the irradiation-damaged microstructures, in conjunction with the typical high-temperature properties of 9% Cr steels, is

that the operating temperature window of Eurofer97 and other RAFM structural components will be limited to ~350-550 °C [3,26]. The lower temperature limit is imposed due to the well-known irradiation-induced low temperature hardening-embrittlement (LTHE) that causes a positive shift of the ductile-brittle/fracture toughness transition temperature [17,27,28], indicating the loss of fracture toughness. LTHE starts at very low doses (~0.1-0.2 dpa) and typically saturates around ~15-20 dpa [8,17]. Literature also suggests a non-negligible deleterious contribution of helium on LTHE [17,28,29], that may prevent LTHE saturation with neutron dose [30]. LTHE is a major challenge especially for the water-cooled blanket DEMO design where the operating temperatures in the range of ~280-350 °C are expected [31]. In the absence of irradiation, the strength of Eurofer97 and other RAFM steels monotonically decreases with increasing temperature [32,33]. Due to LTHE in irradiation environments, increase in strength of RAFM steels occurs for irradiation temperatures (T_{irr}) < 400 °C (particularly pronounced for T_{irr} < 350 °C), whereas minimal hardening is observed near 450-500 °C and some slight softening may occur for T_{irr} > 500 °C [6,15,17,28,34–40]. There are some conflicting data scatters regarding the effect of T_{irr} on incremental radiation hardening, particularly in the temperature range ~250-330 °C. Some studies have reported comparable or decreased radiation hardening in this temperature range [17,36,41–43], whereas some other studies have reported nonmonotonic T_{irr} dependence with maximum hardening for T_{irr} ~300 °C [44–46]. Some of these inconsistencies between different studies may be associated with differences in the dose-dependent hardening up to 5-10 dpa at the different irradiation temperatures. Further, numerous neutron irradiation studies on RAFM steels in literature only provide the “design irradiation temperatures”, but lack actual thermometry data and neutron flux distribution data across samples. Differences between actual versus design temperatures in neutron irradiations and neutron flux inhomogeneities across samples are well-known to occur, which will contribute to scatter in the measured properties.

The upper temperature limit on Eurofer97 and RAFM steels is imposed due to thermal softening and poor creep strength at temperatures higher than ~500-550 °C [26,36,46], which will be exacerbated by irradiation [27]. This is a concern for helium or dual-cooled DEMO designs where the blanket operating temperatures around 600-700 °C are envisaged [47,48]. Improvements in Eurofer97 steels' high-temperature strength has recently been demonstrated by tuning the alloying chemistry and processing routes [49–53]. However, LTBE may be exacerbated with materials tuned for elevated temperature operations because it is often observed that fracture toughness reduces by strengthening means such as lower tempering temperatures/times, cold working and precipitation [8,35,54,55].

The undesirable narrow operating temperature window envisaged for Eurofer97 steel is a significant fusion reactor design challenge. Particularly, the LTBE phenomenon is not only a risk for DEMO where ~20 dpa is expected in the first phase operations [56,57], but also for ITER Test Blanket Module (TBM) activities where the envisaged exposure conditions are limited to ≤ 3 dpa and 300 °C [56]. Early pioneering research in the US on FM steels by Klueh et al. [58,59] has highlighted that improvement of the steels' mechanical properties with potential for better irradiated LTBE behavior can be achieved by alternate thermo-mechanical treatments (TMTs). The Japanese fusion materials development activities on F82H steel, which shows very similar properties to Eurofer97 and also holds one of the largest database for neutron irradiated properties for benchmarking other RAFM steels, has shown that fracture toughness can be improved by finely tuning the chemistry such as in the “mod3” variant [35]. In this context, EUROfusion program produced ten Eurofer97 steel variants using a combination of different minor alloying chemistries and manufacturing-processing routes. These alloys, in non-standard metallurgical conditions, were developed to target better fracture toughness (softer steels) and improved high-temperature strength (harder steels) as compared to Eurofer97 steel in the reference state. At ORNL, fusion relevant neutron irradiations using

the High Flux Isotope Reactor (HFIR) were performed on the Eurofer97 steel variants of the EUROfusion program to screen and quantify the irradiated properties. By taking advantage of small specimen test technology (SSTT) development [60], the irradiations were performed on miniature SS-J3 flat tensile samples targeting ITER-TBM relevant conditions of ~ 3 dpa/300 °C, followed by post-irradiation examination (PIE). Previously, fracture toughness testing performed on miniature 4-notch Charpy bend bar (M4-CVN) specimens of the neutron irradiated EUROfusion steels revealed the transition temperature shifts (ΔT_{0Q}) of these materials [15], while a brief overview of room temperature tested properties and some nanoscale microstructure data can be found in Rieth et al. [61]. In this paper, building from our previous reported data in Ref. [15,61,62], we further extend our analysis of the mechanical property degradation in Eurofer97 steel variants after neutron irradiation using Vickers microhardness indentation tests, uniaxial room/elevated temperature tensile tests and fractography. Specifically, using the experimental results, the research presents the various aspects of the science of deformation and mechanical property degradation to help better understand irradiation hardening in RAFM steels and its potential implications on alloy design strategies. The research compares irradiation hardening in different Eurofer97 variants detected by indentation tests to well-known results in F82H steel and welds, quantifies the irradiation induced loss of strain-hardening, and discusses the irradiated behavior of the tested materials on true stress units where the plastic instability stresses are compared against fracture stresses and yield stress. Additionally, by quantifying the fracture surfaces, we provide an analysis of the reduction in area, which revealed its peculiar correlation to the uniaxial properties.

2. Materials and Methods

2.1 Materials

Ten Eurofer97 steel variants (code names: H, I, J, K, L, M, N, O, P and E) were studied. The thermo-mechanical treatment (TMT) conditions and the material compositions of the steels

are provided in Table 1 and Table 2, respectively and are previously presented in Ref. [61,63,64] . To summarize:

(i) Material E is the reference Eurofer97/2 steel, heat 993391, having the standard chemistry. However, it was received at ORNL after a ‘technological treatment’ [61] that targets simulating atypical situations such as after welding or during problematic manufacturing-processing steps [61]. The material experienced an additional normalization at 980°C followed by a very slow furnace cooling to room temperature (RT) over 24 hours. Then, the standard heat treatment with normalization at 980°C and tempering at 760°C was performed.

(ii) Materials H, I and P, designed at KIT, consisted of varying alloying chemistries in terms of carbon, manganese, vanadium, and nitrogen concentration as compared to the reference state. The steels were tempered at a much higher temperature of 820 °C. Consequentially, the as-received H, I and P steels were relatively softer. More details about these materials can be found in Hoffman et al. [49].

(iii) Material L, designed at CEA, was prepared using a combination of high normalization temperature and low tempering temperature compared to the reference heat treatment conditions of Eurofer97. This steel was much harder than Eurofer97 in the reference state [51,63,65], and has demonstrated significantly improved high temperature creep properties [51]. Relatively recent results have shown this steel to consist of four nanoprecipitate families: $M_{23}C_6$, M_7C_3 , M_2X (Cr rich nitrides) and MX carbo-nitrides [51,66], instead of primarily $M_{23}C_6/MX$ found in Eurofer97.

(iv) A similar high normalization and low tempering temperature approach, but in conjunction with reduced manganese, lower carbon and chromium contents was used for material K designed at SCK-CEN. Material J was also designed at the same lab and was nearly identical to Eurofer97 in chemistry, but with higher oxygen content and a noticeably lower normalization temperature. Further details can be found in Ref. [50].

(v) Materials M and N were produced by double austenization by ENEA. Material M was identical in chemistry to reference Eurofer97, while N had lower manganese, lower nitrogen and no vanadium. Material O, also made by ENEA, was produced by hot-rolling at 650 °C followed by tempering. In addition, this steel consisted of lower carbon and tantalum content, but higher nitrogen, silicon and oxygen concentration compared to the reference Eurofer97. Further details are available in Refs. [53,67].

The starting microstructures of the steels were revealed after mechanical polishing followed by etching using Vilella's reagent and light optical microscopy (LOM). A detailed report of the LOM images, along with further analysis using scanning electron microscopy (SEM), analytical scanning transmission electron microscopy (STEM) and mechanical properties of all the ten steels in the unirradiated state are summarized in Bhattacharya et al. [63].

Table 1: Summary of steel processing conditions. AQ: air quenched, AC: air cooled, WQ: water quenched, Q&T: quenched and tempered, LT: low temperature application, HT: high temperature application, TMT: thermo-mechanical treatment. Adapted from Refs. [61,63,65].

| Material | Material type | Heat | Condition | Provider |
|----------|---------------|--------|--|----------|
| E | EUROFER97/2 | 993391 | Technological treatment: 980°C + slow AC + 980°C/0.5h + AQ + 760°C/1.5h + AC | KIT |
| H | EUROFER-LT | J362A | TMT: 1150°C and then rolling in 8 steps down to a finish rolling temperature (FRT) of 900°C with a reduction of 16% per rolling step, then WQ. 1000°C/0.5h + WQ + 820°C/2h + AC | |
| I | EUROFER-LT | J363A | | |
| P | EUROFER-LT | J361A | | |
| J | EUROFER-LT | I196C | TMT:1250°C/1h and then rolling to FRT of 850°C in 6 rolling steps with a reduction of 20-30% per rolling pass, then AC. Q&T: 880°C/0.5h+WQ+750°C/2h+AC | SCK.CEN |
| K | EUROFER-HT | J427A | TMT:1250°C/1h and then rolling to FRT of 850°C in 6 rolling steps with a reduction of 20-30% for each rolling pass, then AC. Q&T: 1050°C/15min + WQ + 675°C/1.5h + AC | |
| L | EUROFER97/2 | 994578 | 1150°C/0.5h + AQ + 700°C/1.5h + AC | CEA |

| | | | | |
|---|-------------|--------|---|-------|
| M | EUROFER97/2 | 993391 | 1020°C/0.5h + AQ + 1020°C/0.5h + AQ +760°C/1.5h + AC (double austenitization) | ENE A |
| N | EUROFER-LT | VM2897 | 920°C/1.5h + AQ + 920°C/1.5h + AQ + 760°C/1h + AC (double austenitization) | |
| O | EUROFER-LT | VM2991 | TMT: 1080°C/1h, cooling to 650°C and rolling, reduction 40% (from 30 to 18 mm) Tempering: 760°C/1h + AC | |

Table 2: Chemical compositions of different Eurofer97 steel variants. All values are in wt.%. The chemistry of materials E and M was equivalent to a standard Eurofer97. Main elements that differed from a standard Eurofer97 in the derived steel variants are color coded. Table adapted from Refs. [63,65]. Green = values significantly higher than reference Eurofer97. Purple = values significantly lower than Eurofer97.

| Element | Eurofer97 chemistry E and M | H | I | P | J | K | L | N | O |
|-------------------|-----------------------------------|---------|---------|---------|---------|---------|--------|---------|---------|
| Cr | 8.83 | 8.70 | 8.73 | 8.70 | 9.00 | 7.84 | 9.14 | 9.04 | 8.80 |
| C | 0.11 | 0.06 | 0.11 | 0.11 | 0.11 | 0.02 | 0.11 | 0.09 | 0.06 |
| Mn | 0.53 | 0.02 | 0.02 | 0.02 | 0.40 | 0.02 | 0.54 | 0.11 | 0.50 |
| V | 0.20 | 0.35 | 0.35 | 0.20 | 0.22 | 0.22 | 0.20 | <0.05 | 0.30 |
| N | 0.019 | 0.047 | 0.042 | 0.045 | 0.022 | 0.022 | 0.040 | 0.002 | 0.070 |
| W | 1.08 | 1.07 | 1.08 | 1.14 | 1.10 | 0.99 | 1.11 | 0.99 | 0.97 |
| Ta | 0.12 | 0.10 | 0.09 | 0.09 | 0.11 | 0.13 | 0.12 | 0.09 | 0.05 |
| Si | 0.04 | 0.04 | 0.04 | 0.03 | 0.006 | <0.04 | 0.03 | 0.04 | 0.15 |
| S | 0.001 | 0.001 | 0.001 | 0.002 | 0.001 | 0.001 | 0.004 | 0.001 | 0.003 |
| B | <0.0005 | <0.0005 | <0.0005 | <0.0005 | <0.0005 | <0.0005 | 0.001 | <0.001 | <0.001 |
| Ti | <0.0001 | <0.0001 | <0.0001 | <0.0001 | <0.0001 | <0.0001 | 0.001 | <0.01 | <0.01 |
| O | 0.004 | 0.002 | 0.005 | 0.004 | 0.007 | 0.004 | <0.001 | <0.004 | 0.006 |
| Nb | <0.0004 | <0.0004 | <0.0004 | <0.0004 | 0.0070 | 0.0070 | 0.0040 | <0.0100 | <0.0100 |
| Mo | 0.001 | 0.001 | 0.001 | 0.001 | 0.0002 | 0.001 | 0.002 | <0.01 | <0.01 |
| Ni | 0.003 | 0.004 | 0.004 | 0.006 | 0.007 | 0.004 | 0.010 | <0.02 | <0.02 |
| Cu | 0.007 | 0.008 | 0.007 | 0.008 | 0.0007 | 0.008 | 0.003 | <0.01 | <0.01 |
| Al | 0.0012 | 0.0017 | 0.0014 | 0.0016 | 0.0051 | 0.0034 | 0.002 | <0.01 | <0.01 |
| Co | 0.0017 | 0.0017 | 0.0017 | 0.0021 | 0.0041 | 0.0011 | 0.003 | <0.01 | <0.01 |
| As, Zr, Sn, Sb | x | x | x | x | <0.004 | <0.004 | <0.007 | <0.005 | <0.005 |
| P | x | x | x | x | 0.0020 | 0.0031 | 0.0015 | <0.005 | <0.006 |

2.2 Unirradiated optical microstructures of the materials

Light optical microscopy (LOM) images of the ten steels obtained after etching in Villela's reagent are provided in Fig. 1, and more such details for the purpose of comparison can be found in Ref. [61]. The imaging was specifically performed on the rolling direction - normal direction (RD-ND) plane to reveal any processing induced morphological texture of the grains. All the steels showed a tempered martensitic structure with laths, blocks, prior austenite grains (PAGs), and precipitates decorating the laths and PAGBs as represented by the dark etching contrast in Fig. 1.

Materials H, I and P consisted of an over-tempered microstructure (Fig. 1a-c). These steels contained ferrite grains which appeared relatively bright and clear of the black dots (precipitates) in the etched samples. Some ferrite grains are highlighted using yellow arrows in Fig. 1. The over tempered structure is attributable to the relatively high tempering temperature of 820 °C as opposed to typical 740-760 °C tempering for conventional and reduced activation 9% Cr steels [8,10,68]. Material H appeared to have relatively larger grain sizes as compared to I and P. Material J showed a much finer structure with smaller grain sizes such that detecting the PAGs in the optical images was challenging. The finer grain size is expected due to the lower normalization temperature of 880 °C [50,61]. Materials K and L showed the largest PAGs among all the steels, as evident in Fig. 1e-f. The very large PAG sizes in both K and L are expected due to the high normalization temperature of 1050 and 1150 °C, respectively, instead of typical 980 °C for a standard Eurofer97. To better reveal the grain structure of these two steels, lower magnification optical images are shown in Fig. 2 where the PAGBs in both these steels are recognizable.

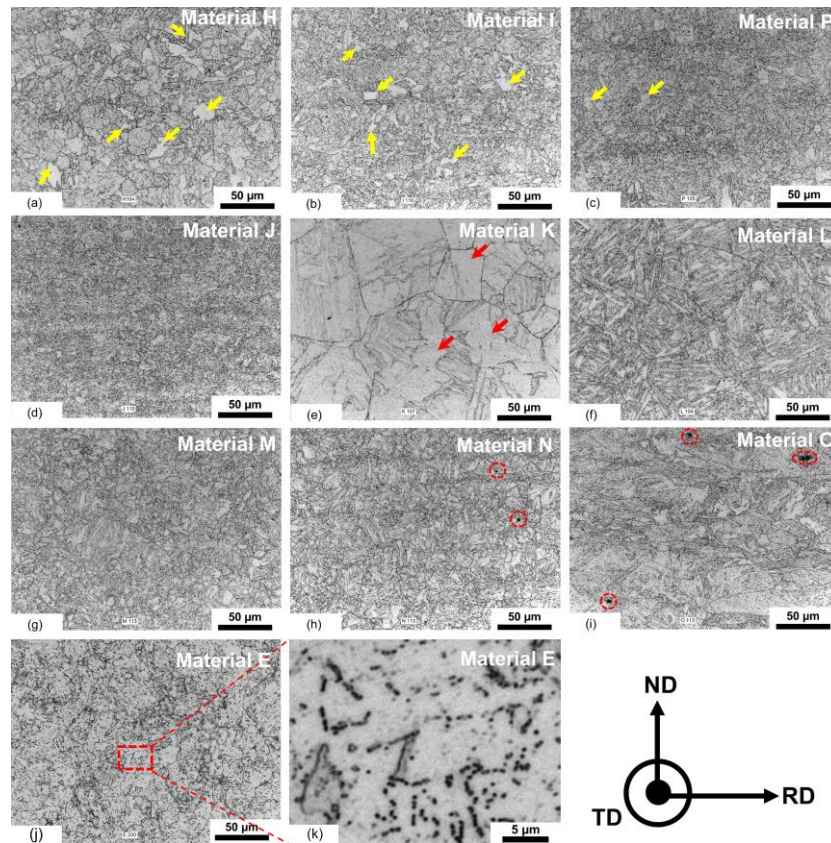


Fig. 1: LOM images of the as-received EUROfusion steels after etching in Vilella's reagent. (a, b, c) KIT materials: H, I and P, (d, e) SCK-CEN materials: J and K, (f) material L from CEA, (g, h, i) ENEA materials M, N and O, (j) material E. (k) Higher magnification image of material E showing coarse precipitates detected at optical μm length scales. Yellow arrows point to ferrite grains in H, I and P. Red arrows point to areas in material K where no lath structure was visible. Dotted red circles show inclusions detected in materials O and N. ND = normal direction, RD = rolling direction and TD = transverse direction. More LOM images of these steels can be found in Ref. [61].

Material L consisted of a well-developed lath structure and uniformly sized PAGs, while material K appeared to show a mixed population of large ($>50\text{-}60\ \mu\text{m}$) PAGs in addition to evenly distributed smaller $<40\ \mu\text{m}$ size grains. However, a well-developed lath-type martensitic structure was not clearly evident in the optical images for material K where numerous regions devoid of laths were detected after etching, indicated by red arrows in Fig. 1e and visible throughout in Fig. 2a. This might be due to a combination of lower C content and a significantly lower tempering temperature (under-tempering) for this material. Materials M and N, which were double austenized, showed a fine tempered martensitic structure. Some inclusions were detected in material N, which were identified as Ta rich, and are expected to

be oxides as reported in Ref. [63]. Material O consisted of elongated grains along the rolling direction as evident in Fig. 1i. This is expected because of plate rolling TMT at temperature as low as 650 °C, without austenization (see Table 1). Similar to material N, Ta-rich inclusions were also detected in material O [63].

The optical images of material E are provided in Fig. 1j-k. The microstructure was typical tempered-martensitic. However, numerous coarse precipitates and their clusters were detected (Fig. 1k) in the material. The presence of coarse precipitates was verified by SEM and analytical STEM characterization reported in Refs. [63,65]. These precipitates most probably formed during the slow AC (furnace cooling) step and didn't fully dissolve during the second normalization step. Additionally, these precipitates are also expected to coarsen during tempering. The grain structure of material E also appeared relatively coarser, which is evident when comparing with material M that was identical in chemistry to material E. Previously, Charpy tests on material E in the unirradiated state reported no significant adverse effects of the coarse precipitates on the impact properties [61]. However, Chen et al. [15,65] noted significantly higher T_{0Q} FT transition temperature for material E in unirradiated and irradiated states using miniature bend bar specimens, that was attributed to the starting coarse precipitates.

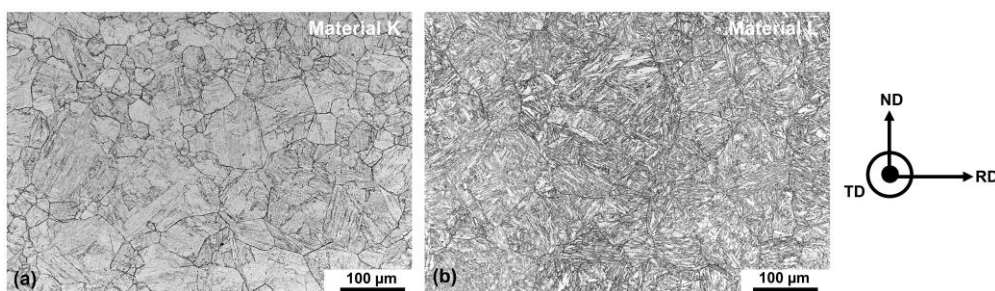


Fig. 2: Lower magnification LOM images of (a) material K and (b) material L after etching.

2.3 Neutron irradiations

Neutron irradiations were performed in the flux trap rabbit facility of the 85 MW_{th} mixed spectrum HFIR at ORNL, targeting 2.5-3 dpa at 300 °C. For bracketing the desired irradiation temperature of 300 °C, two rabbit capsules were designed with target temperatures

of 285 ± 20 °C and 315 ± 20 °C. Type SS-J3 flat tensile specimens having the dimensions: 16 mm (length) x 4 mm (width) x 0.75 mm (thickness) and gauge dimensions of 5 mm (length) and 1.2 mm (width) were irradiated inside sealed non-instrumented rabbit capsules commonly known as GENTEN capsules [69]. The capsules were inserted in HFIR cycle 477A (4 days) and stayed in for cycle 477B (20 days) and cycle 478 (24 days) for a total of 48 days in-pile irradiation which corresponded to ~ 4063 MWD (megawatt days) at nominal operating power. Four samples per material, amounting to a total of forty SS-J3 samples were irradiated, with twenty samples inside each capsule. The accumulated fast neutron fluence ($E > 0.1$ MeV) in the two capsules was relatively similar: 4.15×10^{25} n/m² and 4.57×10^{25} n/m². Using a displacement threshold energy of 40 eV for Fe and Cr, the estimated doses corresponding to the fast fluences were 2.94 and 3.24 dpa, respectively. The average axial fast flux variation for the two radial positions used in the HFIR flux trap and the fast flux variation across the two capsules are shown in appendix A. The center of the two rabbit capsules was located ~ 5 cm above and ~ 7 cm below the horizontal midplane of the reactor, thereby providing relatively flat neutron flux (and dpa) axial profile with less than $\sim 7\%$ variation from the top to bottom of the capsules. The samples were held in three smaller cylindrical holders located inside each capsule. Because the length of an SS-J3 sample/holder is significantly smaller as compared to the length of a capsule, the neutron flux/dose variation along the length of a single SS-J3 sample was $< 2\%$ (see appendix A). In addition to SS-J3 samples, the capsules contained a total of twenty-four SiC thermometry pieces (twelve inside each capsule) for sample irradiation temperature estimation. More details about the irradiation capsule geometry, including the arrangement of the samples inside the capsules, are provided in the Supplementary Materials. Further details about HFIR neutron flux distribution can be found Refs. [70,71].

2.4 Capsule and specimen temperature control

The specimen temperatures inside the capsules depend upon the axial location inside the reactor, holder material, fill gas and gap size between the specimen holder and outer housing. The specimens were held inside capsules constructed from aluminum alloy 6061 with helium as the filler gas. The temperature contour plots of the SS-J3 samples predicted using finite element modeling (FEM) by the HFIR design team [69,71] are provided in the appendix B, which show uniform calculated temperatures across the gauge length, and the temperatures of the opposing grip sections constant within $\pm 10\text{-}15$ °C. In addition to FEM modeling, passive SiC thermometry analysis was performed after irradiation to measure the capsule temperature distribution using the dilatometry based standard procedures [72]. The SiC thermometry results, overlaid with capsule loading schemes, are provided in the Supplementary Materials. Moreover, the estimated temperatures of each tensile sample are tabulated in the Supplementary Materials, where exact sample ids are reported for future traceability using ORNL's hot-cell database. Because SiC thermometers were located relatively internal to the capsule with respect to the samples (see loading scheme in Supplementary Materials), the measured thermometry represents the maximum temperature in the capsule. Thus, final sample irradiation temperatures (T_{irr}) must be estimated by combining experimental passive thermometry with input from FEM. Using this methodology, T_{irr} of forty samples in two rabbit capsules ranged between $\sim 255\text{-}350$ °C, and all these samples were tested by Vickers hardness to investigate the effect of T_{irr} on irradiation hardening in the temperature range. Only the samples showing T_{irr} in the range of 300 ± 30 °C were tensile tested to compare irradiation hardening/ductility loss since the measured irradiation hardening by indentation testing appeared to be independent of irradiation temperature within this temperature range (see section 3.1.1).

2.5 Post irradiation examination at ORNL hot- cells

Vickers microhardness indentation tests were performed at room temperature on all the irradiated samples in accordance with ASTM E384 Standard Test Method for Microindentation Hardness of Materials, using 1 kg load and 15 s dwell time. Among other things, this standard mainly imposes the restriction on distance between the indents and the distance between an indent and the sample edge: both must be minimum $2.5dV$, where dV represents the average Vickers diagonal distance. These tests were conducted using a Mitutoyo HV-120B hardness tester. The indentations were made before performing tensile tests on the two grip sections of SS-J3 tensile specimens. All forty neutron irradiated samples were tested with a minimum of six indents and up to twelve indents per sample (a total of 240 – 480 measured indents), spread across the two grip sections, to provide an average hardness value of each steel. For nonirradiated steels, a total of 82 samples were tested with minimum six indents per sample. In absence of a heating furnace attached to hardness machine in the hot-cells, the tests were performed at room temperature (RT).

Uniaxial tensile tests were performed at RT and 300 °C on the subset of samples with $T_{irr} \sim 300 \pm 30$ °C with guidance from ASTM E8 Standard Test Methods for Tension Testing of Metallic Materials and ASTM E21 Standard Test Methods for Elevated Temperature Tension Tests of Metallic Materials using a strain rate of 10^{-3} s^{-1} ($5 \times 10^{-3} \text{ mm/s}$ extension rate). The tangent modulus method was used to provide accurate values for the yield strength and uniform and total plastic elongations from the measured crosshead displacement in the absence of gauge extensometry for miniature tensile samples. Using machine crosshead displacement introduces additional elongation in the pseudo-elastic regime due to machine and load-train compliance effects, but it does not affect the plastic regime or the calculated strength values when these parameters are measured using the tangent modulus offset plastic deformation method. The specimens were shoulder loaded for testing using an Instron 5967 tensile machine equipped with a 5kN load cell and connected with an Instron Bluehill3 analysis software. This tensile

machine is equipped with an Oxy-Gon tungsten mesh furnace capable of reaching 1200 °C. RT tests were performed in air. Elevated temperature tests were performed in vacuum at pressures $\leq 5 \times 10^{-6}$ torr. For tensile tests at 300 °C, the temperatures were measured using two thermocouples welded onto the fixture. The temperature ramp-up time from room to test temperature was typically between ~25-30 minutes. The tests were performed only when the sample temperature stabilized to the set-point of 300 ± 5 °C. During the data analysis, efforts were devoted to remove the machine slack during the initial loading portion in the experimentally observed stress-strain curves. Fractography was performed on the broken pieces of SS-J3 samples tensile tested at RT and the reduction in area was quantified. A tungsten filament-based JEOL JSM-6010LA scanning electron microscope (SEM) was used to record the fracture surface images using a secondary electron detector.

3. Results and discussion

3.1 Quantifying irradiation hardening by Vickers hardness indentation tests

3.1.1 Temperature effect on irradiated hardness

Vickers microhardness indentation tests were performed on all the forty irradiated SS-J3 samples. The hardness results as a function of T_{irr} are plotted in Fig. 3. The results are separately presented for the harder steels (K and L) and the relatively softer steels (E, H, I, P, J, M, N, O). Fig. 3 indicates the measured microhardness was constant within error bars for each studied alloy; i.e., there was no statistically detectable dependence of irradiation temperature on incremental radiation hardening in the range of $T_{\text{irr}} \sim 255\text{-}320$ °C. As mentioned in the introduction section, literature on RAFM steels typically show a scatter in irradiation hardening for irradiation temperatures between ~250-300 °C, with some conflicting data showing either slight increase or slight decrease in irradiation hardening in this temperature range [28,36,41,44]. Over a wider temperature range of $T_{\text{irr}} \sim 200\text{-}350$ °C, a moderate decrease in hardening with increasing irradiation temperature is typically observed for RAFM steels.

The most prominent effect of irradiation temperature in RAFM steels is typically around ~350-375 °C where hardening should reduce as compared to lower T_{irr} values [17,28,36,43], and DBTT should improve drastically. In our case, for T_{irr} ~340-350 °C, hardness of steels did not reduce significantly as compared to the values measured at lower irradiation temperatures (Fig. 3). Results from European neutron irradiation campaigns such as SPICE program also show remnant irradiation hardening in reference Eurofer97 when $T_{irr} = 339 - 354$ °C (≥ 150 MPa detected by tensile testing, $T_{test} = RT$)[73], which is qualitatively consistent with our results highlighting that irradiation hardening around ~350 °C does not fully recover as compared to lower irradiation temperatures ($T_{irr} \leq 300$ °C). It should be noted that error bars in the irradiated hardness in Fig. 3 slightly complicates identifying moderate hardness recovery trends, if any. The error bars originated from the statistical variability in the measured values. The result from every test, performed on the two grip sections of forty SS-J3 samples, are additionally provided in appendix C. It is worth noting that the relatively large error bars on hardness for some samples in Fig. 3, such as for material E irradiated close to 330 °C and material N close to 345 °C, originated from differences in the measured hardness between one grip section to the other of the same tensile sample, where one end tab exhibited higher hardness (by about ~70 -120 HV) compared to the other. This may be an indication of moderate irradiation temperature gradient between the two end tab regions in these specimens (in this case a lower irradiation temperature than the average value, due to some enhanced heat transfer for this end tab). These samples, such as exact sample ids E294, N110 in appendix Fig. A3, were excluded from any further analysis, but for the sake of completeness the data points are still provided in Fig. 3. Additionally, the SiC thermometry method used in our study has an uncertainty of ± 20 °C when compared with thermocouple measurements or from differences in the analysis algorithms, as reviewed by Field et al. [74]. If the recovery of hardness is sharp around $T_{irr} \geq 350$ °C, the empirical ± 20 °C error range with SiC thermometry and any potential small fluctuation of the

sample temperatures towards lower values could result in relatively harder steels. Therefore, higher irradiation temperature data will be needed to confirm when hardening will subside in these Eurofer97 variants. One other point to note is that unlike many other materials test reactors, HFIR always operates at constant power [75]. Therefore, power-induced temperature fluctuations of the specimens and holder material over the ~24 day reactor core lifetime are minimal in the HFIR flux trap [75]. For our study, the full set of thermometry data for the EUROfusion tensile rabbit capsules are discussed in detail in Ref. [62]. Owing to a general lack of neutron data for $T_{irr} < 220-250$ °C for Eurofer97 type steels, what remains unclear is the hardening behavior at lower irradiation temperatures. Correlating the temperature dependent irradiated strengths of other FM steels such as MANET-I [76] and F82H [8,77] suggests that hardening should be more pronounced for $T_{irr} < 200$ °C, with maximum hardening expected when T_{irr} reaches RT.

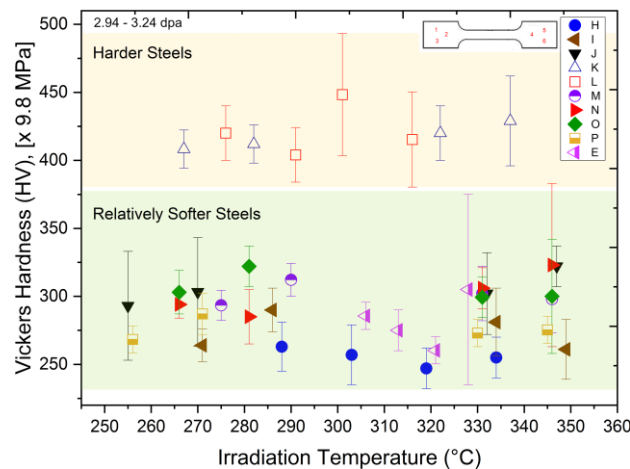


Fig. 3: Vickers microhardness as a function of the irradiation temperature of the Eurofer97 type steels after neutron irradiations to 2.94 – 3.24 dpa. Inset shows a SS-J3 schematic (not to scale) of the general pattern of the indentation testing. A ± 20 °C range for T_{irr} is estimated for the irradiation temperatures in this figure based on recommendations in Refs. [72,74].

3.1.2 Irradiation-induced Vickers hardness increase and comparison with F82H: $T_{irr} \sim 300 \pm 30$ °C

For specimens with $T_{irr} = 300 \pm 30$ °C, the irradiated hardness is compared against the unirradiated samples, and with literature on F82H-IEA steel and F82H joints irradiated in

HFIR to similar T_{irr} /neutron doses using same sample geometries [78] (Fig. 4). The F82H-IEA steel shows almost identical properties to reference Eurofer97 in unirradiated condition, due to which the irradiated properties of both these steel types are also expected to similar [17,79]. Moreover, the database of neutron irradiated properties of F82H for benchmarking purposes is also considerably larger than Eurofer97. The change in hardness is plotted in Fig. 4b, while the percentage increase in hardness due to irradiation, calculated as $[(HV_{irradiated} - HV_{unirradiated})/HV_{unirradiated}] \times 100\%$ is plotted in Fig. 4c. All the steels hardened significantly after neutron irradiations. The percentage change in Vickers hardness of different materials ranged between ~25% to 40%. Materials K and L were the hardest in the unirradiated state owing to low tempering temperatures. After irradiation, these two steels remained significantly harder, exceeding 400 HV (~3.92 GPa). All the other steels showed irradiated hardness between ~250-300 HV (2.45-2.94 GPa). It is worth noting that Figs. 4a-b suggest that material K shows the highest hardness increase in terms of absolute numbers. However, when the values are expressed in the percentage change in hardness, i.e. change with respect to the starting state, the difference between most materials was not very different as the data points were within the error bars (Fig. 4c). Therefore, solely by Vickers microhardness indentation tests, it is complex to judge which steel performed better. Even for material K, it was evidently clear that despite having larger absolute change in hardness value, the percentage hardening was not vastly different as compared to other steels. Therefore, material K should not be considered as showing highest radiation hardening. This highlights that expressing radiation hardening only on the absolute scale can be often prone to misinterpretation, especially when comparing hardening between vastly different materials that have significant differences in their starting properties. Expressing the data on the normalised percentage scale is more suitable, especially for identifying best performing alloys. This is because two steels with very different starting hardness (such as softer and a harder material) could show similar hardness increase due to

irradiation, but they should not be mistakenly considered as showing similar hardening behavior. As will be shown in the next section, this point is also valid when comparing the irradiated tensile properties.

The relative change in hardness due to irradiation between all Eurofer97 variants and F82H steels/welds was similar, which suggests that the irradiation hardening behavior of these materials is quite alike. It remains to be seen if this trend will continue or will deviate significantly at elevated neutron doses.

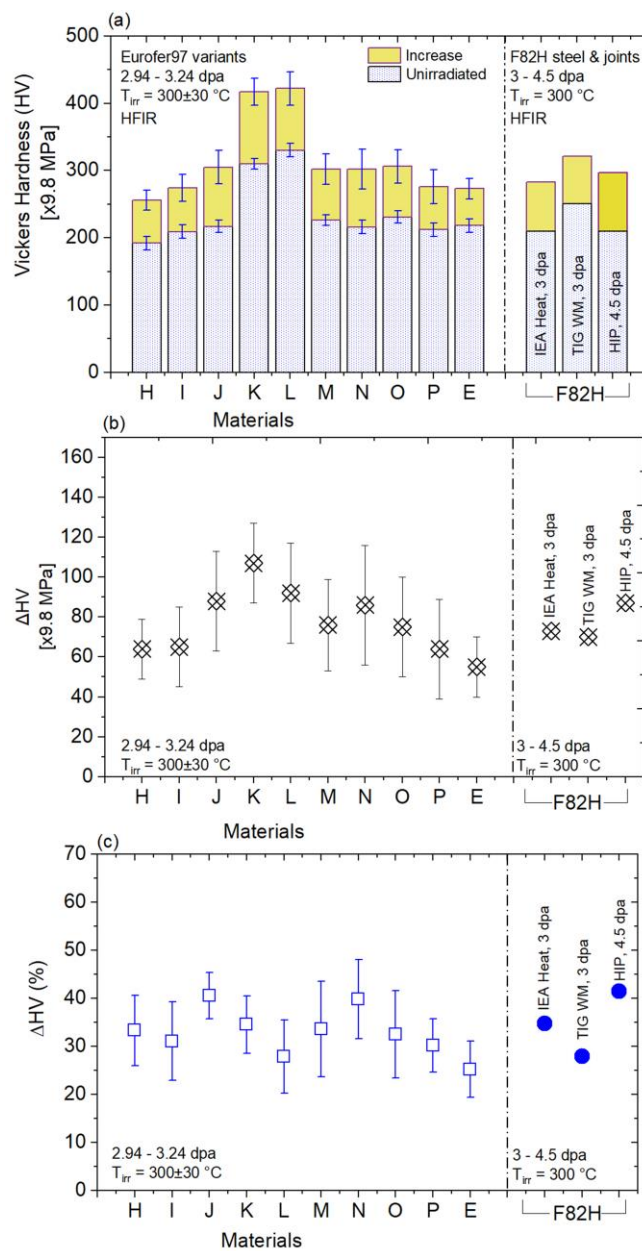


Fig. 4: Vickers microhardness after HFIR neutron irradiations at 300 ± 30 °C, 2.94 - 3.24 dpa. (a) Comparing unirradiated and irradiated hardness of the ten Eurofer97 steel variants and F82H steel/welds. (b) Increase in microhardness due to irradiation. (c) Percentage increase in microhardness. IEA = International Energy Agency, TIG WM = tungsten inert gas weld metal, HIP = hot-isostatic pressed joints. F82H data adapted from Ref. [78].

3.2 Quantification of irradiation hardening and ductility loss by tensile testing

Using a strain rate of 10^{-3} s⁻¹, tensile tests were performed on the SS-J3 samples at RT and 300 °C. The engineering stress-strain curves from the irradiated and unirradiated specimens are shown in Fig. 5. Further, the σ_{YS} , ultimate tensile stress (σ_{UTS}), and tensile elongation before and after irradiation are presented in Fig. 6. A summary of the quantitative results is tabulated in appendix D (Tables A1 and A2). In agreement with the indentation hardness results, the experiments revealed that all the steels hardened profusely after neutron irradiation, with significant increase of σ_{YS} and σ_{UTS} . This was accompanied by loss of tensile ductility, shown by degradation of uniform plastic elongation (UE_p) and total plastic elongation (TE_p). Further, as an example, a comparison of the irradiated stress-strain curves for $T_{irr} = 268$ °C and $T_{irr} = 330$ °C is given in supplementary materials (Fig. S4, material N), where we did not see a major effect of T_{irr} on the tensile properties, which broadly confirmed the hardness results.

The primary ductility remaining in all the steels was post necking ductility with little UE_p . This is consistent with literature on neutron irradiated conventional FM steels and RAFM steels in the LTBE regime (for $T_{irr} < 350$ °C) where post σ_{UTS} necking elongation is known to be the dominant contributor [8,10,46,80]. For $T_{test} = RT$, the UE_p of the irradiated steels shown in Fig. 6 reflect a little improved irradiated properties as compared to previous studies in Eurofer97, because the elongation of baseline Eurofer97 is known to be severely reduced even for very low neutron doses. For example, previous rabbit capsule based HFIR neutron irradiations on Eurofer97 miniature flat tensile specimens to 1.5 dpa, 300 °C had revealed UE as low as 0.2% [81]. In fact, the UE of neutron irradiated Eurofer97 is well-known to reduce

with dose and saturate with values consistently lower than 0.4-0.5% for $T_{irr} \sim 300 \text{ }^\circ\text{C}$ [44,82]. However, there seems to be some discrepancy in the literature about when UE saturation occurs in RAFM steels with results from Lucon et al. [44] showing saturation at doses as low ~ 0.6 - 0.7 dpa, whereas the compilation of 300 - $325 \text{ }^\circ\text{C}$ irradiated tensile properties by Alamo et al. [83] showing saturated UE ($< 0.5\%$) occurring at higher doses (>3 - 4 dpa). Low dose (0.08 – 0.1 dpa) F82H data irradiated in Japan Research Reactor-2 (JRR-2) reports UE $> 0.5 \%$, with values around 2.5% and TE around 14.5% for $T_{irr} = 300 \text{ }^\circ\text{C}$ [84]. The fact that UE_p is higher than typical saturation values below 0.5% for most steels in Fig. 6 seems to suggest saturation may not have been reached yet in our experiments. The TE_p of all the irradiated steels for $T_{test} = RT$ ranged between ~ 12 - 17% . These irradiated TE_p values are generally consistent with previous neutron irradiation data on RAFM steels, including Eurofer97, for doses less than 4-5 dpa [83]. In general, the loss of TE in Eurofer97 type steels is known to worsen with dose, but saturates around ~ 10 - 12 dpa at values close to ~ 9 - 10% [83]. For the irradiation doses in the present study, we expect the saturation of TE may also not have been attained yet.

The strength and elongation behavior of the ten steels was dependent upon the test temperature. The strength of the unirradiated and irradiated steels was lower for elevated temperature tensile testing, which is expected. However, the steels showed reduced ductility for $T_{test} = 300 \text{ }^\circ\text{C}$. This behavior is normal for Eurofer97 type steels [82], and is attributed to dynamic strain ageing (DSA) [55,85] in which the dislocation glide motion can be obstructed by the Cottrell atmosphere formed around the interstitial elements like carbon and nitrogen that follow the stress fields created by the moving dislocations [86]. Consequentially, the dislocations become less glissile due to the constant pinning-unpinning motion from the interstitial atoms, which is generally known to reduce ductility in metals [87]. Previous results from fracture toughness testing of FM steels such as HT9 suggest that neutron irradiation mitigates the DSA effect [55,87,88]. The present results show that the potential DSA behavior,

inducing lower tensile ductility at higher test temperatures, was present in most of the Eurofer97 steel variants after the low dose neutron irradiations (Fig. 6c-d).

Here, we re-emphasize the point that the elastic load-up portion of the load vs. crosshead displacement curves suffer from machine compliance effects which must be analyzed using tangent modulus methods to obtain correct tensile elongation data (see appendix D). The elastic elongation of RAFM steels is typically very small ($\sim 0.3\%$ at yielding for a yield stresses of ~ 700 MPa), which means uniform elongation (UE) $\sim UE_p$ and total elongation (TE) $\sim TE_p$. The plastic region of the stress-strain curves is unaffected by compliance or load train slack [89]. All the elongation data presented and discussed in this manuscript reports the plastic component of the elongation. For more detailed strain analysis in the elastic region and plastic flow localization phenomena, measurements using the digital image correlation (DIC) method recently developed at ORNL for hot-cell operations [89] are required for future irradiation campaigns.

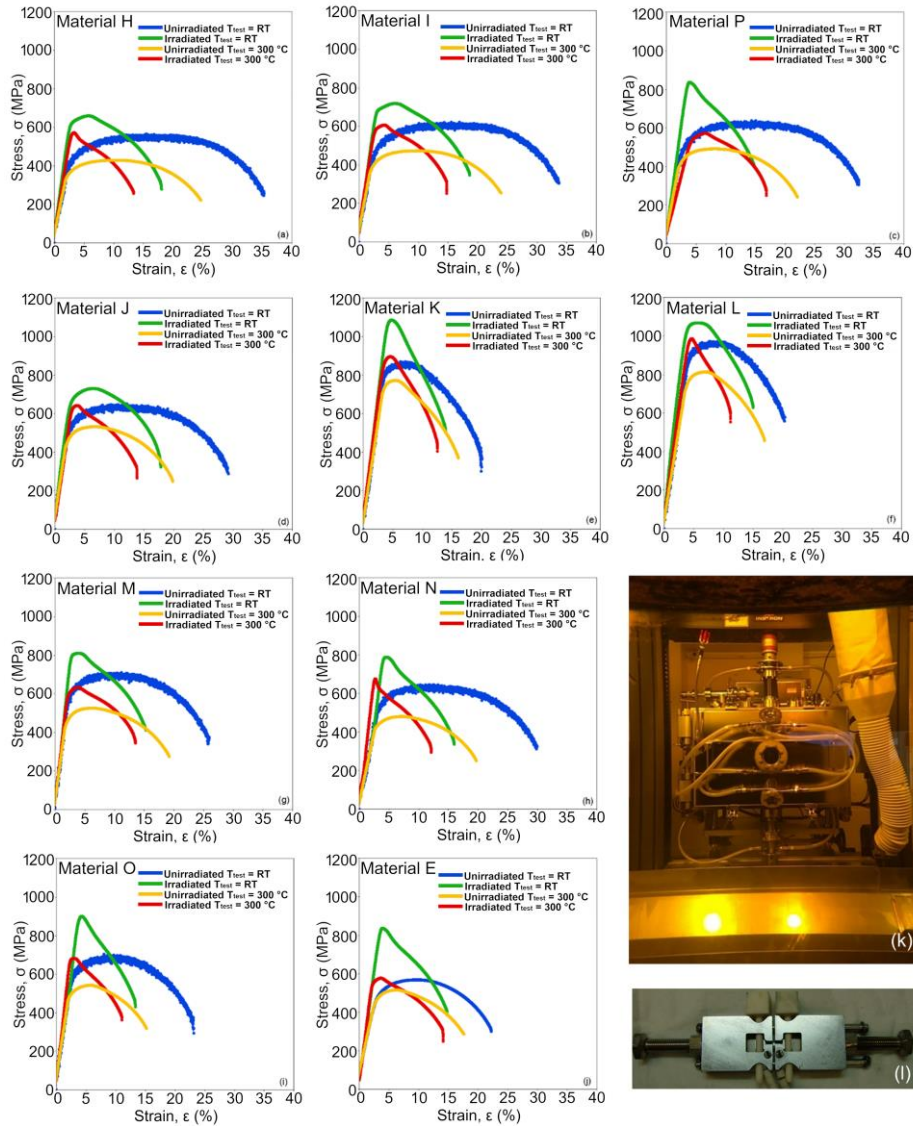


Fig. 5: Engineering stress-strain curves of the Eurofer97 steel variants after HFIR neutron irradiation to 2.94 – 3.24 dpa, 300±30 °C, compared against the unirradiated control samples. Tests performed at RT and 300 °C. The hot-cell tensile machine and the fixture used for testing are shown in (k) and (l), respectively.

Fig. 6 also includes the RCC-MRx minimum limits imposed for unirradiated Eurofer97 tensile properties at RT [90,91], where its comparison with the irradiated results is presented. In the unirradiated state, materials H, I and E were softer than the minimum RCC-MRx strength limits for $T_{\text{test}} = \text{RT}$. The σ_{YS} and σ_{UTS} of materials J, N and P were close this limit, M and O were slightly harder, while K and L were significantly harder. After irradiation, all the steels became significantly harder than the minimum code limit for $T_{\text{test}} = \text{RT}$. Even for $T_{\text{test}} = 300 \text{ }^\circ\text{C}$, most irradiated steels were harder than the unirradiated RCC-MRx limits of Eurofer97 [91]. In

terms of TE_p , most materials after irradiation were close to the minimum limit at RT as seen in Fig. 6d, but materials H, I and J performed better. However, particularly for comparing UE, caution must be taken because some differences in measurements between flat samples (especially miniature and with absence of contact extensometer) and cylindrical cross-sections samples are expected [92]. Presently, RCC-MRx does not contain a section with irradiated Eurofer97 properties.

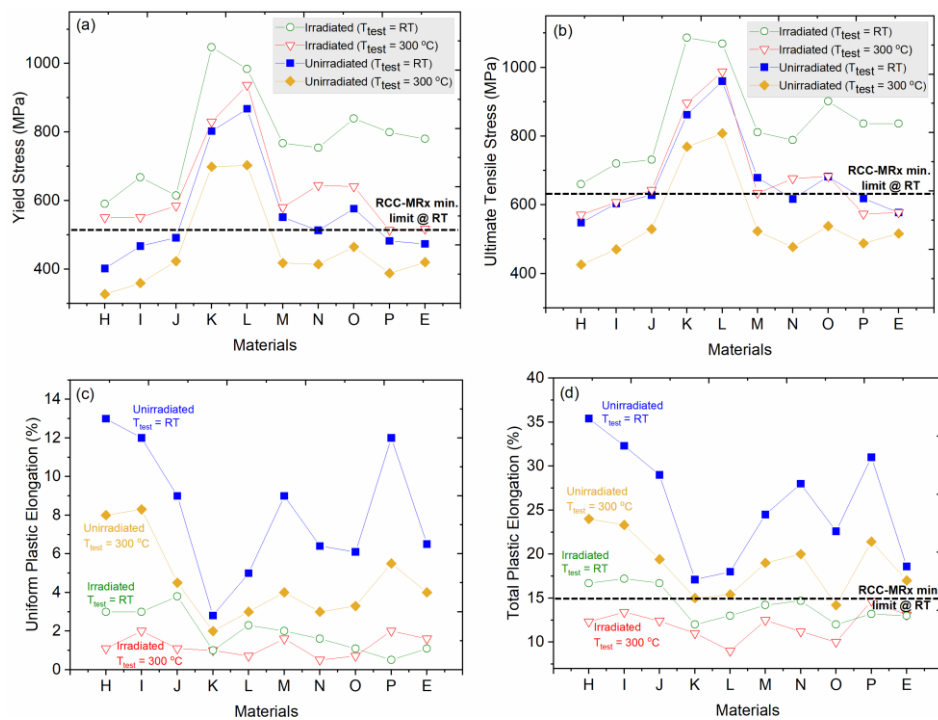


Fig. 6: Tensile properties comparison of the ten Eurofer97 steel variants before and after HFIR neutron irradiation to 2.94 – 3.24 dpa, $300\pm 30\text{ °C}$. (a) σ_{YS} (b) σ_{UTS} , (c) UE_p and (d) TE_p . The RCC-MRx limit lines, taken from Refs. [90,91], are added for the unirradiated reference Eurofer97 steel. Strength data from RT tests adapted from Ref. [61].

By comparing the RT tested unirradiated and irradiated samples, the percentage gain in σ_{YS} , σ_{UTS} and the associated percentage loss in elongation of the ten steels are plotted together in Fig. 7. The change in σ_{YS} or σ_{UTS} was calculated by the expression $\Delta\sigma = [(\sigma_{irradiated} - \sigma_{unirradiated})/\sigma_{unirradiated}] \times 100\%$, while the loss in tensile ductility was calculated by $\Delta UE_p = [(UE_p)_{irradiated} - (UE_p)_{unirradiated}]/(UE_p)_{unirradiated} \times 100\%$ and $\Delta TE_p = [(TE_p)_{irradiated} - (TE_p)_{unirradiated}]/(TE_p)_{unirradiated} \times 100\%$. The percentage increase in σ_{YS} ($\Delta\sigma_{YS}$) varied significantly between the different steels, ranging from as low as ~13% to values as high as

66% (Fig. 7a). Highest percentage $\Delta\sigma_{YS}$ at RT, with values $>60\%$, was shown by materials P and E. Specific to material E, due to the ‘technological heat treatment’ (980°C followed by very slow air-cooling), it had consisted of coarse carbides, formed through high temperature diffusion without martensite formation [61]. Further, a homogeneous distribution of fine precipitates, as expected in Eurofer97, was also not obvious for material E [61,63]. Collectively, these microstructure features likely resulted in the lower unirradiated strength and poor post-irradiation hardening for this material. The tensile properties of material E are consistent with the results showing poor post-irradiation fracture toughness of this material after irradiation to same dose-temperature in HFIR, with fracture toughness transition temperature (T_{0Q}) much higher than room temperature [15]. As pointed out by Rieth et al. [61], the technological heat-treatment to produce material E rather covers the lower range of Eurofer97 properties, and is an approximation for heat-treated weld joints after irradiation or for steel batches produced with potential production issues. The most obvious influence on hardening is detected for steels fabricated with higher normalization temperatures and lower tempering temperatures that consisted of under-tempered microstructures and simultaneously consisting of large prior austenite grains (materials L and K in the present study). Such steels are significantly harder in the unirradiated state – contribution to material L’s higher hardness may also originate from higher N concentration while material K had very low C that is expected cause W to stay in solid-solution adding to hardness (but causing poor fracture properties) [61]. After irradiation, these steels showed relatively low percentage increase in σ_{YS} and σ_{UTS} as compared to most softer steels. The relatively harder L series steel showed the least increase in σ_{YS} due to irradiation, at 13.3%. This might be explained due to a combination of two factors. Firstly, material L consisted of a high density of nanoprecipitates in the starting microstructure, such as the finely dispersed M_2X precipitates in addition to the presence of MX precipitates [51,66]. Consequentially, the sink strength of this material is expected to be

somewhat higher than other steels. It is well-known that $\Delta\sigma_{YS}$ due to neutron irradiations is lower for steels having higher sink strength due to high nanoprecipitate densities [4]. A second more logical reason that could contribute to lower $\Delta\sigma_{YS}$ is that the unirradiated Vickers hardness and σ_{YS} of material L (also material K) was already high. Therefore, the possibility to further harden such steels under irradiation is smaller as compared to relatively softer steels – irrespective of the minor alloying chemistry. The phenomenon of initially harder steels showing smaller $\Delta\sigma_{YS}$ is also observed in neutron irradiated F82H produced by different tempering temperatures and times [93].

Although there is a spread in $\Delta\sigma_{YS}$ for the ten steels, the initially large strength increase at low neutron doses is qualitatively consistent with literature on RAFM steels [8,16,94,95]. In terms of elongation loss, the harder steels (materials K and L) and material J showed relatively lower UE_p loss (Fig. 7b), while the percentage UE_p loss of other materials was worse, ranging between $> -75\%$ and up to -96% as compared to their unirradiated state. Qualitatively, a similar trend existed for ΔTE_p (Fig. 7b). But ΔTE_p was smaller than ΔUE_p for most steels, further highlighting the importance of necking ductility. It is worth pointing out that a steel with very high unirradiated UE_p and TE_p could lose elongation significantly and may still retain acceptable tensile ductility, whereas little changes to elongation due to irradiation for a steel with only a few percent unirradiated elongation can be severely consequential. Therefore, the relatively low loss of elongation for alloys K and L should not be interpreted as a highly favorable result because the low ΔUE_p and ΔTE_p is a consequence of these alloys starting with a relatively low elongation, so they have a relatively low possible further loss in elongation. The initially harder steels, such as materials L and K, typically show poor fracture properties during fracture toughness testing, as revealed by Chen et al. [15], where both steels showed fracture toughness transition temperature T_{0Q} significantly higher than room temperature after neutron irradiation to same conditions as in the present study. Material J stands out because it

showed relatively low degradation of the tensile properties due to irradiation - in terms of low $\Delta\sigma_{YS}$ increase, and relatively low ΔU_{Ep} and ΔTE_p values. Based on literature, material J also has better fracture properties after similar irradiations conditions, with T_{0Q} of $-58\text{ }^{\circ}\text{C}$ as compared to $+48\text{ }^{\circ}\text{C}$ for L and $+137\text{ }^{\circ}\text{C}$ for K [15]. This overall better performance is expected owing to the relatively finer PAG sizes in this material due to normalization at a lower temperature ($880\text{ }^{\circ}\text{C}$), as compared to all other steels. In addition, relatively lower Mn compared to Eurofer97 and much lower Si concentration in J is also expected to produce a lower fraction of irradiation induced Mn-Si co-clustering as revealed in Refs. [22,96] that can deleteriously effect the LTBE behavior in both conventional FM and RAFM steels. The irradiated hardness/tensile properties of other steels, such as those obtained by simultaneous chemistry changes (reducing carbon and manganese, increasing/decreasing vanadium and nitrogen) combined with double austenitization, low-temperature rolling (elongated grains) and tempering at higher temperatures (over-tempered microstructure + ferrite grains) does not seem to differ significantly in terms of irradiation behavior. It is likely that the steel microstructures produced by changes in micro-chemistry seems to influence the irradiated tensile properties. However, changes in the heat treatment/processing appears to have a stronger effect [61].

A standard Eurofer97 was not included in the present irradiation campaign. Therefore, a direct comparison with the reference material is difficult. However, literature suggests that Eurofer97 may experience roughly $\sim 220\text{-}300\text{ MPa}$ increase in σ_{YS} after neutron irradiations to somewhat similar irradiation conditions [17,18,28,44]. When comparing with the ten steels in the present study it seems most steels show similar range of absolute change in σ_{YS} (values provided in Supplementary Materials). Materials that clearly stand out are L and J with absolute change in σ_{YS} of 116 MPa and 124 MPa respectively. It is important to note that most of the standard Eurofer97 neutron irradiated data is derived from irradiations on relatively large cylindrical cross-section samples [17], while the present results are obtained from miniature

samples. Therefore, any comparison here with standard Eurofer97 data should be viewed with caution due to potential size effects. While the size effect may be less problematic for comparing strength values, the elongation values between SSTT specimens and large specimens can often vary. Here, we would also like to highlight that similar to the comments in the Vickers hardness section, measuring the changes in σ_{YS} on the absolute scale, i.e., $\Delta\sigma_{YS} = (\Delta\sigma_{YS})_{\text{irradiated}} - (\Delta\sigma_{YS})_{\text{unirradiated}}$, can erroneously depict two materials with vastly different irradiated tensile properties as having similar hardening behavior. As an example, this can be seen for materials K and N where both show increase of σ_{YS} around 240-245 MPa due to irradiation (see Fig. 6a and Supplementary Materials). However, material K was much harder than N in the unirradiated state. Therefore, the increase in σ_{YS} of material K with respect to its initial properties is a much lower fraction as compared to N. Therefore, caution must be taken when hardening behavior of steels with different starting properties is compared. This problem can be addressed if $\Delta\sigma_{YS}$ due to irradiation is expressed in the normalized percentage scale as in Fig. 7. On the percentage scale, the data point in literature by Lucon et al. [41] suggest that ~40-45% increase in σ_{YS} of standard Eurofer97 may occur after neutron irradiations at ~300 °C /~2-2.5 dpa. Based on this data, it seems J, K and L show relatively less hardening.

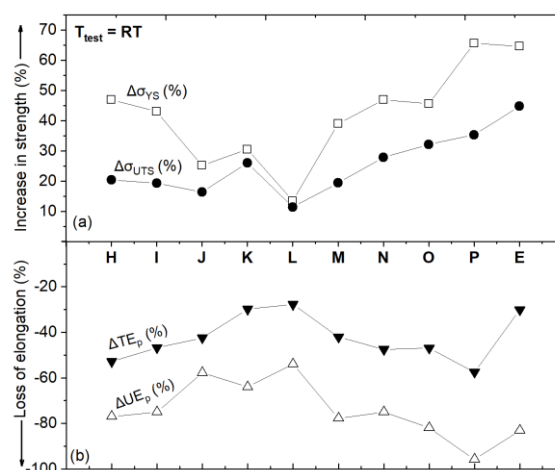


Fig. 7: Relative comparisons of the irradiation hardening and loss of ductility of the ten Eurofer97 steel variants after neutron irradiations to 2.94 – 3.24 dpa. (a) Percentage increase in σ_{YS} , σ_{UTS} , due to neutron irradiation. (b) Percentage loss of uniform and total plastic elongation.

3.3 Comparison of strain hardening capacity of the Eurofer97 steel variants

A parameter of key importance for structural steels in fusion blanket designing is the strain hardening capacity. From engineering stress-strain curves, a fair representation of strain hardening capacity of RAFM steels can be approximated as the σ_{UTS}/σ_{YS} ratio for a given tensile test temperature. Ideally, the σ_{UTS}/σ_{YS} figure of merit as high as possible is desirable. In general, body centered cubic (bcc) steels such as RAFM steels are not known to strain harden significantly as compared to austenitic steels. For example, in the entire temperature range relevant for ITER-TBM operation, Eurofer97 exhibits a much lower strain hardening capacity as compared to 316L austenitic steels in the unirradiated state, with σ_{UTS}/σ_{YS} ratio progressively worsening with test temperatures [82]. Therefore, quantifying the strain hardening capacity of neutron irradiated Eurofer97 type steels under reactor relevant conditions is essential. In Fig. 8, the σ_{UTS}/σ_{YS} ratios of the ten irradiated steels for $T_{test} = RT$ and $300\text{ }^{\circ}C$ are compared.

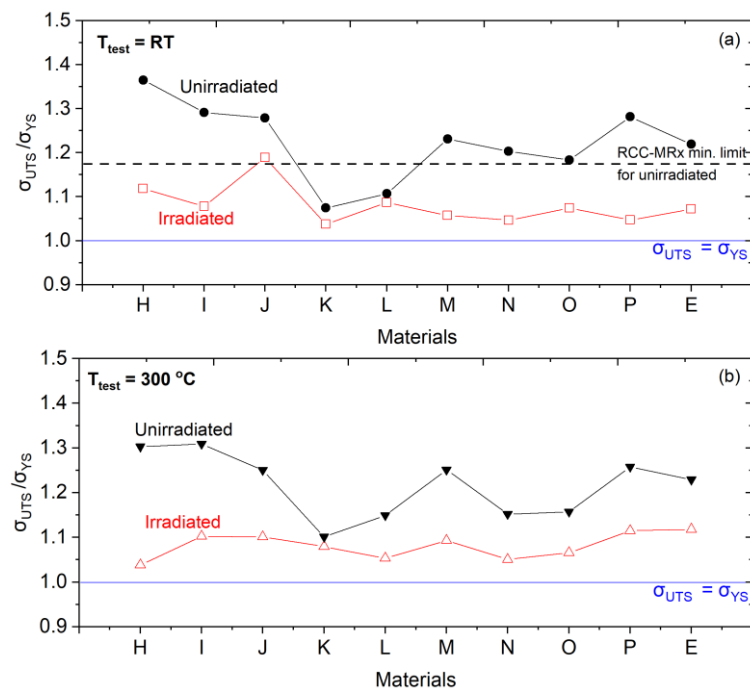


Fig. 8: Strain hardening, estimated as the ratio of σ_{UTS} and σ_{YS} of the ten Eurofer97 steel variants before and after neutron irradiation to 2.94 – 3.24 dpa, $T_{irr} = 300\text{ }^{\circ}C$. (a) Tensile tests at RT. (b) Tensile tests at $300\text{ }^{\circ}C$. The RCC-MX/MRx limit on σ_{UTS}/σ_{YS} ratio at RT adapted from Ref. [82] for the unirradiated Eurofer97 is overlaid in (a).

The RCC-MX/MRx σ_{UTS}/σ_{YS} minimum limit for unirradiated Eurofer97, extracted from Aiello et al. [82] for $T_{test} = RT$, is overlaid in Fig. 8a. For the unirradiated samples, most steels showed σ_{UTS}/σ_{YS} at RT equal to or better than the minimum requirement laid out in RCC-MX/MRx. The harder low temperature tempered K and L steels behaved in a relatively poor manner, showing significantly lower σ_{UTS}/σ_{YS} ratios with values ≤ 1.1 at RT. After irradiation, strain hardening capacity of all the steels degraded. Most steels showed $\sigma_{UTS}/\sigma_{YS} < 1.1$ for both $T_{test} = RT$ and $300\text{ }^{\circ}C$. Best performance was shown by material J because even in the irradiated state it showed σ_{UTS}/σ_{YS} ratio at RT slightly better than the unirradiated RCC-MX/MRx minimum limit. We expect the strain hardening capacity to worsen with neutron dose as σ_{YS} continues to increase until saturation around $\sim 12\text{-}15$ dpa for $T_{irr} \sim 300\text{-}330\text{ }^{\circ}C$ [8,10,17]. Overall, the combined results using tensile and hardness tests reflect that different metallurgical modifications made to Eurofer97 such as changing minor alloying chemistry, changing fabrication-processing route, and simultaneously modifying heat treatment makes only minor improvements in the LTHE susceptibility of Eurofer97. While improvement in UE_p at RT with values up to 3.8% after ITER-TBM relevant irradiations was achieved in material J, other steels still suffered from a severe lack of uniform tensile ductility. Further, high temperature tests at $300\text{ }^{\circ}C$, that are more engineering relevant, show negligible improvements in UE_p in all the experimental alloys in this study with values consistently lower than $\sim 1\text{-}2\%$.

3.4. Comparing irradiated Vickers microhardness and tensile properties

The σ_{UTS} and microhardness from all the irradiated steels are scatter plotted in Fig. 9. The results followed a linear trend, giving the relation $\sigma_{UTS} \sim \alpha HV$ at RT, where $\alpha = 2.7$. This is consistent because Vickers hardness in HV unit (kg/mm^2) scales linearly with σ_{YS} and σ_{UTS} in Fe-based alloys [37,97,98]. As visible in Fig. 8, RAFM steels do not typically retain much strain hardening capacity after neutron irradiations around $300\text{ }^{\circ}C$. Therefore, the value of α is not expected to change much if σ_{YS} was used. The results agree well with the strength-hardness

relationship of unirradiated and irradiated RAFM steels, and conventional tempered martensitic steels in literature where values for α between 2.6-3.5 are reported [37,65,98,99].

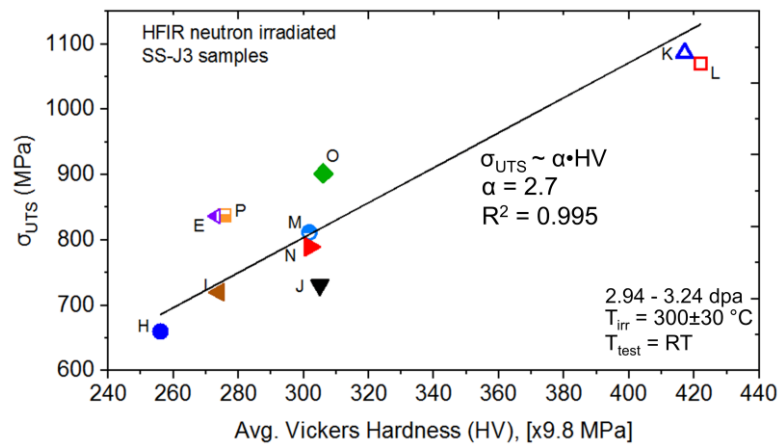


Fig. 9: Relationship between σ_{UTS} and average Vickers microhardness of the neutron irradiated Eurofer97 steel variants.

3.5 Understanding the material behavior in terms of true stress

The irradiation hardening behavior of metallic materials can be further understood if the tensile results are compared in true stress units. The true stress can be obtained from engineering stress using the relation $\sigma_{true} = \sigma_{eng} \exp(\epsilon)$, where ϵ is true strain [100]. The true stress converted from σ_{UTS} is defined as the true stress at maximum load. This true stress is also called the plastic instability stress σ_{PIS} [100,101], which has been reported to be constant for a given material and is independent of neutron dose [101]. Therefore, the margin between σ_{PIS} and σ_{YS} is an indicator of the materials' real work hardening capacity. If $\sigma_{YS} \geq \sigma_{PIS}$, no uniform deformation will occur and plastic instability onset will cause prompt necking at yield [101]. In Fig. 10, σ_{PIS} versus σ_{YS} of the ten irradiated Eurofer97 steel variants are plotted for $T_{test} = RT$. All the steels were in the region where $\sigma_{PIS} > \sigma_{YS}$, implying some uniform deformation capability was remaining after irradiation. Further, all the steel variants had roughly similar work hardening margins after irradiation. However, the σ_{YS} of most steels was very close to the “ $\sigma_{PIS} = \sigma_{YS}$ ” line. This implies any further small σ_{YS} increase, such as with additional dose, will completely exhaust the capability of these steels to uniformly deform. Materials J and L, lying

further away from the “ $\sigma_{PIS} = \sigma_{YS}$ ” line, showed relatively better performance as compared to the other steels.

For improving the irradiation hardening/loss of ductility, Fig. 10 implies that alloy designing should target producing materials with a large separation between σ_{PIS} and σ_{YS} , so that the materials can have a large work hardening margin and uniform deformation capability after irradiation. In other words, the improvements in σ_{PIS} should not be achieved at a cost of highly increased σ_{YS} , as observed in Fig. 10 for materials L/K. Material L seems to have more attractive features compared to K because it has higher σ_{PIS} relative to its σ_{YS} . Worst case scenarios for alloys would occur if materials lie in the grey shaded area of Fig. 10 where failure would occur without any uniform tensile ductility.

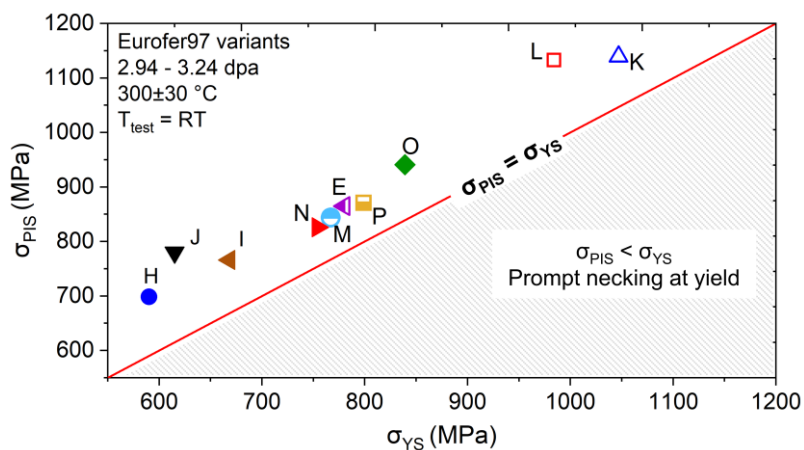


Fig. 10: Comparison of true plastic instability stress (σ_{PIS}) and σ_{YS} of the neutron irradiated Eurofer97 steel variants.

The true fracture stresses (σ_f) of neutron irradiated RAFM steels is another useful quantity to compare the performance of different materials. The σ_f was calculated by dividing the load at fracture by the fracture surface cross-section area measured using an SEM. A comparison of σ_f and σ_{PIS} of the steels before and after irradiation is plotted in Fig. 11a and the σ_f / σ_{PIS} ratios are plotted in Fig. 11b. No significant effect of irradiation on σ_f and σ_{PIS} was noticeable. This is consistent with literature where it is known that: (i) σ_{PIS} of a material is unaffected by irradiation [80,101] and (ii) σ_f of 9%Cr FM steels for $T_{irr} \leq 300$ °C and as low as

80 °C is not much modified by low neutron doses, until significant embrittlement starts for doses ≥ 10 dpa [80]. Material K had the lowest σ_f at values lower than 1000 MPa. The σ_f of all the other steels ranged between $\sim 1000 - 1500$ MPa, which agrees well with low dose (<10 dpa) neutron irradiated data on other bcc steels such as 9Cr-2WVTa, 9Cr-1MoVNb and commercial nuclear alloys such as A533B [80]. The σ_f of most steels was larger than σ_{PIS} , including the σ_f/σ_{PIS} ratios being mostly >1 (Fig. 11). In agreement with similar results in literature [80], this is another direct evidence that most of the total plasticity occurs during necking in neutron irradiated RAFM steels. Consequentially, for a better understanding of the irradiation hardening-embrittlement behavior, the necking deformation in these materials should be given increased attention, including analysing the reduction in area (RA).

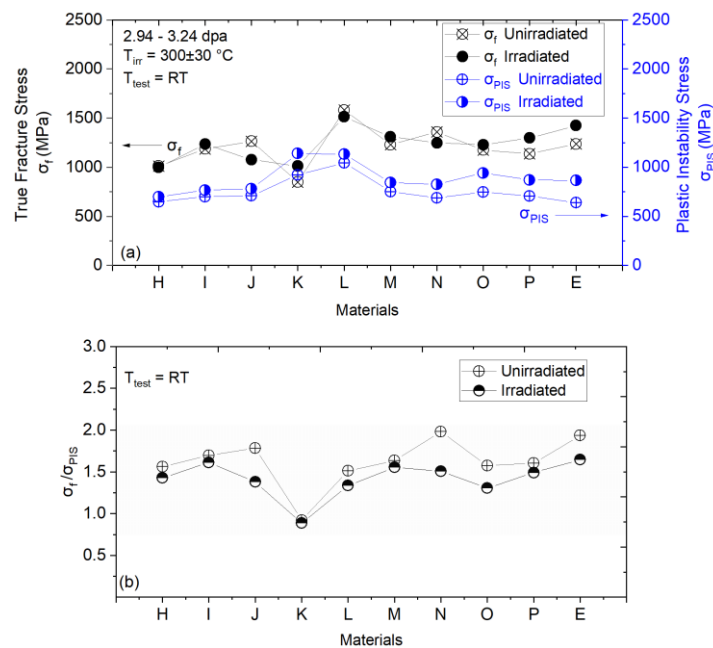


Fig. 11: (a) Comparing true fracture stress (σ_f) and plastic instability stress (σ_{PIS}) of the unirradiated and neutron irradiated Eurofer97 variants. (b). σ_f/σ_{PIS} ratio of the steels.

3.6 Analysis of fracture modes and RA

3.6.1 Characterizing the fracture surfaces

Fractography using SEM was performed to (i) understand the failure modes of the irradiated Eurofer97 steel variants and (ii) to quantify the RA at fracture after tensile testing at RT. Most steels showed ductile cup-and-cone type fracture mode with dimpled surfaces

containing hard inclusions after tensile deformation. Secondary electron images of the fracture surfaces for the ten irradiated steels are presented in Fig. 12. The low temperature tempered K and L steels failed via mixed deformation modes with mostly ductile intragranular fracture, but there were numerous brittle cracks detected. Some brittle fractured areas are highlighted using arrows for material L in Fig. 12. Because the brittle areas primarily appeared planar, we suspect such cleavage failures occurred along the PAGBs or lath boundaries. No evidence of any intergranular brittle fracture was detected in the other steels. The failure mode of material I may also be considered as a mixed fracture mode, because one isolated region showing brittle cleavage was indeed detected. But overall, its failure was ductile. Similar deformation modes of all the steels was reported in the unirradiated samples by Bhattacharya et al. [63], implying irradiation had little effect on the tensile failure modes of these steels. Materials J, N and O had consisted of large oxide inclusions in the steel microstructures [63] and we believe those inclusions generated the relatively large burrow-like cup-and-cone deformed regions visible in Fig. 12c, g and h.

3.6.2 Quantitative comparison of RA

As the previous sections showed, the main ductility remaining in neutron irradiated RAFM steels is during necking. Therefore, quantifying the necking behavior by measuring the RA is highly valuable to better understand the irradiated properties. Further, the conventional understanding is that ductility decreases with increasing strengthening. But this is mainly derived from tensile elongation results and has not been well studied in terms of RA behavior. A comparison of RA before and after irradiation, calculated by quantifying the cross-section area from SEM images for $T_{\text{test}} = \text{RT}$, is shown in Fig. 13. The results reveal RA degraded due to neutron irradiation. Before irradiation, most samples showed RA between ~80-85%, except material L which was close to 75%. After irradiation, RA of most steels reduced to 65-75%, except for material L at ~55%. Despite the irradiation-induced degradation, the RA values of

the steels are relatively large due to large post necking ductility. The results are consistent with previous data available on neutron irradiated Eurofer97 where RA > 65% are typically reported for doses up to ~10-15 dpa at $T_{irr} = 300 \text{ }^{\circ}\text{C}$ [44] and >50% RA for doses up to 70 dpa [102]. This suggests most of the steel variants irradiated in this study are at least comparable to reference Eurofer97 in terms of necking properties. The irradiated RA of the steels in this study are also comparable to results available on F82H neutron irradiated miniature tensile samples, compiled by Zinkle et al. [103].

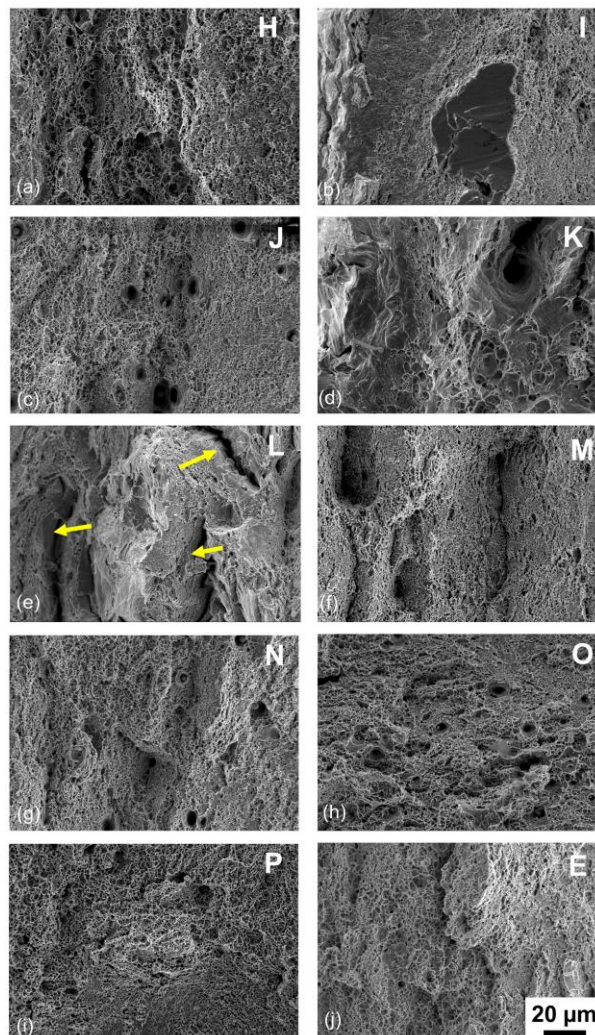


Fig. 12: SEM secondary electron images showing the fracture surface of the ten Eurofer97 steel variants after neutron irradiation to 2.94 – 3.24 dpa at $300 \pm 30 \text{ }^{\circ}\text{C}$. Yellow arrows indicate regions with brittle cracks. Images of E, I and K adapted from Ref. [61].

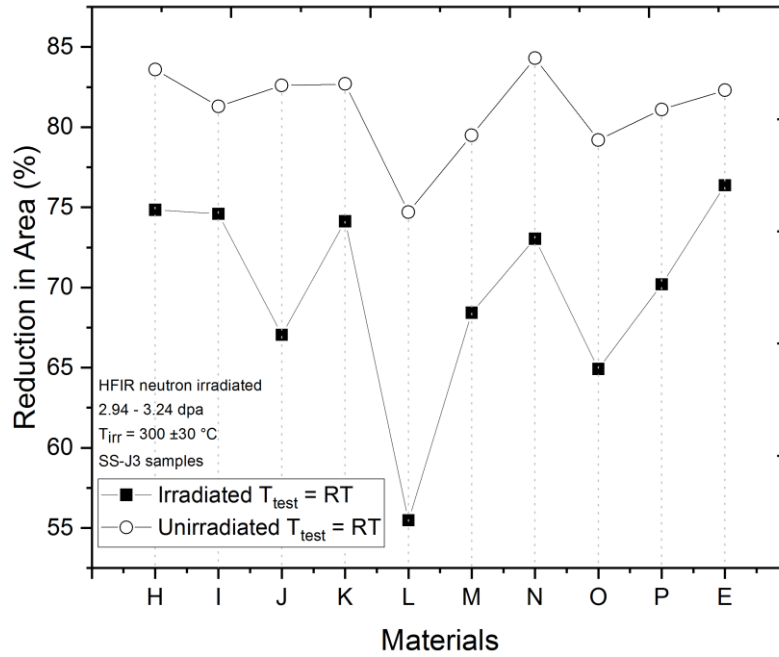


Fig. 13: RA of the ten Eurofer97 steel variants before and after irradiation, measured after RT tensile tests.

To compare the necking behavior in relation to the uniaxial properties, the irradiated σ_{YS} is plotted against irradiated RA for the ten steels in Fig. 14. Additionally, data from other RAFM and conventional FM steels neutron irradiated to similar dose-temperature conditions are also plotted in the same figure. The results reveal that generally the steels with higher irradiated σ_{YS} tend to have lower RA, which is not surprising. An exception to this was material K. However, interesting trends emerged when the loss in RA (ΔRA) due to neutron irradiation is plotted against yield stress increase ($\Delta \sigma_{YS}$) and loss in uniform elongation (ΔUE) in Fig. 15. This figure also contains literature data on 9Cr-1Mo, 9Cr-1MoVNb, F82H and other experimental 9-11%Cr alloys irradiated to similar neutron dose-temperatures [104]. The results revealed that ΔRA and $\Delta \sigma_{YS}$ appeared inversely correlated (Fig. 15a). This suggests that the materials which suffered from the most irradiation hardening showed the least loss of necking elongation and vice-versa, which goes against the conventional wisdom. For example, the Eurofer97 variant L, hardened by only ~116 MPa in the present study, but suffered from >19% loss in RA due to irradiation. On the other hand, material E hardened by >300 MPa, but only showed RA loss of 6%. Data from literature on other FM steels plotted in Fig. 15a also followed

a qualitatively similar behavior, which suggests that the trend is perhaps not a mere coincidence. The ΔRA is plotted against ΔUE for the same materials in Fig. 15b, where a clear trend was not as obvious. However, most Eurofer97 steels from the present study and F82H irradiated in OSIRIS reactor under similar irradiation conditions [104] seems to follow an inverse correlation between ΔRA and ΔUE . The materials not following this general trend were those with already small ΔUE before irradiation, which are the points for $\Delta UE < -2\%$ in Fig. 15b. These results imply that the steels which perform better under irradiation in terms of properties relevant for uniaxial stress conditions (such as σ_{YS} and UE), show relatively poor performance for property changes under triaxial stress states such as in the necking region. A fundamental reason for the interesting trends observed in Fig. 15 is currently unknown but may signify some unaccounted changes in the deformation modes of the irradiated steels as the stress state transforms from uniaxial to triaxial. Specific to ΔUE vs ΔRA comparison, Fig. 15b may imply that UE is sensitive to different material parameters than RA, even though both are measures of ductility. More data on FM steels specifically on RA is needed to further populate Fig. 15 and fine-tune the general trend.

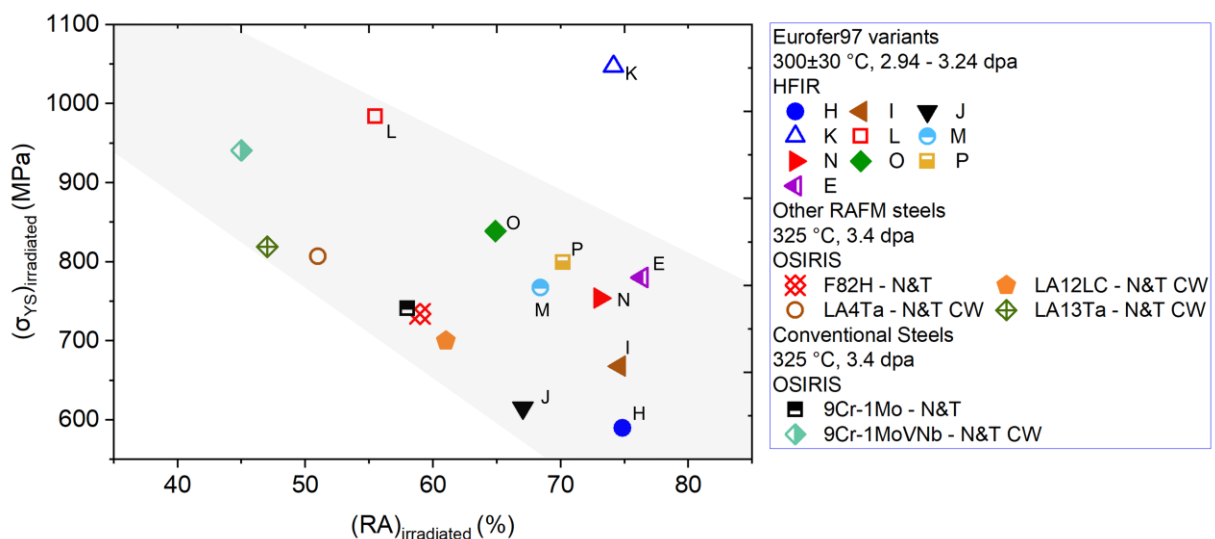


Fig. 14: The irradiated σ_{YS} and RA of the ten HFIR irradiated Eurofer97 steel variants. The data is compared with literature on alloys such as F82H, 9Cr-1Mo based steels and other alloys irradiated in OSIRIS reactor at 325 °C, 3.4 dpa [104]. LA12LC = 9Cr-0.7W alloy, LA4Ta =

11Cr-0.7W-Ta and LA13Ta = 9Cr-3W-Ta alloys. N&T = normalized and tempered, CW = cold worked.

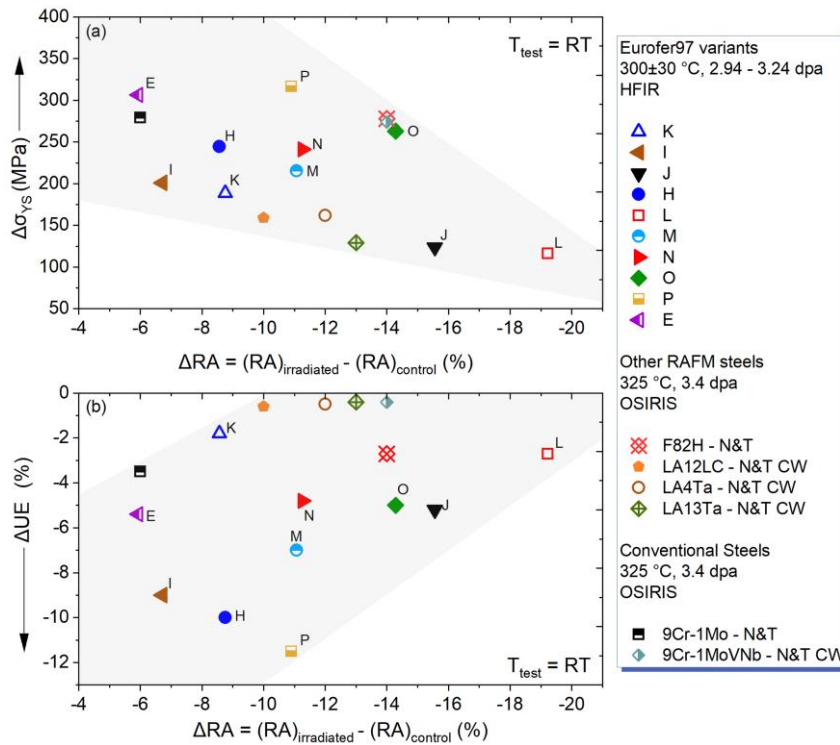


Fig. 15: Loss in RA, taken as the difference between RA for irradiated and unirradiated (control) samples versus (a) increase in σ_{YS} and (b) loss in UE of RAFM and conventional FM steels after neutron irradiations. The data from the present study is compared with literature on F82H, 9Cr-1Mo steels and other alloys irradiated in OSIRIS reactor at 325 °C, 3.4 dpa. LA12LC = 9Cr-0.7W alloy, LA4Ta = 11Cr-0.7W-Ta and LA13Ta = 9Cr-3W-Ta alloys. N&T = normalized and tempered, CW = cold worked. For Eurofer97 variants in the present study, $\Delta UE \sim \Delta UE_p$. $\Delta UE = (UE)_{\text{irradiated}} - UE_{\text{unirradiated}}$.

4. Conclusions

Neutron irradiations in HFIR were performed on ten Eurofer97 steel variants to quantify their low temperature hardening and loss of ductility behavior. The irradiations were performed at ITER-TBM relevant conditions of 2.94 – 3.24 dpa, 255 – 350 °C on SS-J3 type miniature flat tensile specimens. PIE experiments such as Vickers microhardness indentation tests, uniaxial tensile tests and fracture surface analysis quantified the mechanical properties. Tensile tests were performed for samples in the irradiation temperature (T_{irr}) range of 300±30 °C. Following are the main conclusions:

- Similar to results on standard Eurofer97 and other conventional RAFM steels, the Eurofer97 steel variants in non-standard metallurgical condition also suffer from irradiation hardening and loss of ductility, with significant increase in yield stress (σ_{YS}), ultimate tensile stresses (σ_{UTS}) and severe loss of uniform plastic elongation for TBM relevant irradiation conditions of 300 ± 30 °C and ~ 3 dpa. Primary ductility remaining after irradiation is necking ductility.
- The extent of hardening in Eurofer97 variants, measured as increase in σ_{YS} , ranges between $\sim 13\%$ to as high as 66% for the present irradiation conditions. Changes in the heat treatment/processing seems to have a stronger effect than chemistry modification on irradiated properties.
- Harder materials, such as under-tempered microstructures, show relatively low percentage increase in σ_{YS} and σ_{UTS} as compared to most softer steels. These steels also seem to show relatively less degradation of the tensile elongation due to irradiation. This behavior does not imply better properties in terms of tolerance to irradiation hardening/embrittlement. These steels being already much harder in the starting state and having low uniform elongation means the possibility to further harden or lose ductility is lower as compared to softer steels. Such steels will typically show relatively inferior pre- and post-irradiation fracture toughness, despite showing apparently less irradiation-induced degradation of the tensile properties.
- Reduction in area (RA) of Eurofer97 variants degrades with irradiation. However, most steel variants retain sufficient post necking ductility with primarily ductile fracture mode after neutron irradiations and RA between $65-75\%$. Harder steels produced by under-tempering may show some signs of brittle cleavage fracture in addition to the dimpled regions. The results suggest brittle cleavage fracture regions in neutron irradiated under-tempered steels may run along the grain/lath boundaries.

- Similar to the results on other RAFM steels, neutron irradiation significantly exhausts the strain hardening capacity of the Eurofer97 steel variants at $T_{irr} = 300 \pm 30$ °C. The reduced strain hardening capacity after irradiation was inferred from the plastic instability stress (σ_{PIS}) of the steels being only slightly larger than σ_{YS} at room temperature and the σ_{UTS}/σ_{YS} decreasing significantly after irradiation.
- No major effect of irradiation on true fracture stress of the Eurofer97 type steels occurs, which is consistent with literature on neutron irradiated FM steels for doses < 10 dpa. Further, as expected, σ_{PIS} remains largely unaffected by irradiation.
- An inverse relationship seems to exist between loss in RA, loss in UE and increase in σ_{YS} due to neutron irradiations at 300 ± 30 °C.
- In general, the microchemistry modifications such as changes in C, V, N and Mn concentration combined with different fabrication-processing routes used for alloys in this study show only modest improvements in the LTBE susceptibility as compared to irradiation performance of well-studied F82H or baseline Eurofer97. While some alloys show slight improvement in uniform plastic elongation (UE_p) after irradiation (like materials H, I and J), these steels still suffer from a lack of UE_p especially at higher temperatures of 300 °C.
- The present results suggest that RAFM steel development should target materials with a large separation between σ_{PIS} and σ_{YS} , to ensure the materials can maintain large work hardening and uniform deformation capability after irradiation. This research also shows that material J performed the best highlighting that prior austenite grain size refinement is a promising pathway to improve irradiation hardening/loss of ductility behavior, and this strategy should be further investigated to target additional improvements in performance of RAFM steels. This conclusion is further strengthened by the fact that literature shows material J also has better irradiated fracture toughness compared to the rest of the steels.

Processing changes to refine prior austenite grain size might also benefit from low concentration of elements that are prone to radiation induced solute nanoclustering such as Mn and Si that are beginning to be investigated as potential causes of additional hardening in RAFM steels. The strategies to produce initially harder steels does not benefit LTBE. In addition to no improvements in UE_p by increasing unirradiated hardness obtained either by under-tempering or under-tempering combined with microchemistry modification (such as increasing N in material L or lower Cr and very low C in material K that might keep W in solution), these combined processing-chemistry changes seem to make RAFM steels susceptible to some brittle cleavage fracture even during tensile loading conditions where historically standard RAFM steels show fully ductile tensile fractures up to very high doses (70-80 dpa) in absence of He cogeneration. Analytical microstructural characterizations are needed to identify potential effects of irradiation on damage formation to isolate the effect of chemistry from processing on hardening/loss of ductility.

Funding: This study was supported by the U.S. Department of Energy, Office of Fusion Energy Sciences under contract DE-AC05-00OR22725 and Karlsruhe Institute of Technology under contract NFE-16-06240 with ORNL managed by UT Battelle, LLC. A portion of this research at ORNL's High Flux Isotope Reactor was sponsored by the Scientific User Facilities Division, Office of Basic Energy Sciences, US Department of Energy. This work has been carried out within the framework of the EUROfusion Consortium and has received funding from the Euratom research and training program 2014-2018 and 2019- 2020 under grant agreement No. 633053. The views and opinions expressed herein do not necessarily reflect those of the European Commission.

Acknowledgements

The authors thank HFIR team for capsule design, capsule construction, and irradiations. The authors thank Cansu On and Patrick Champlin from ORNL for assistance with neutron flux

profile calculations. Contribution of Clay Morris and operators at ORNL's IMET hot-cell facility in facilitating mechanical testing is sincerely acknowledged. We would like to thank the colleagues who contributed to the development, production, preparation of the different steel grades: L. Malerba (SCK-CEN), C. Cristalli (ENEA), O. Tassa (CSM), J. Hoffmann (KIT) and N. de Wispelaere (OCAS).

Declaration of Interest: None

Appendix A: Fast neutron flux profiles

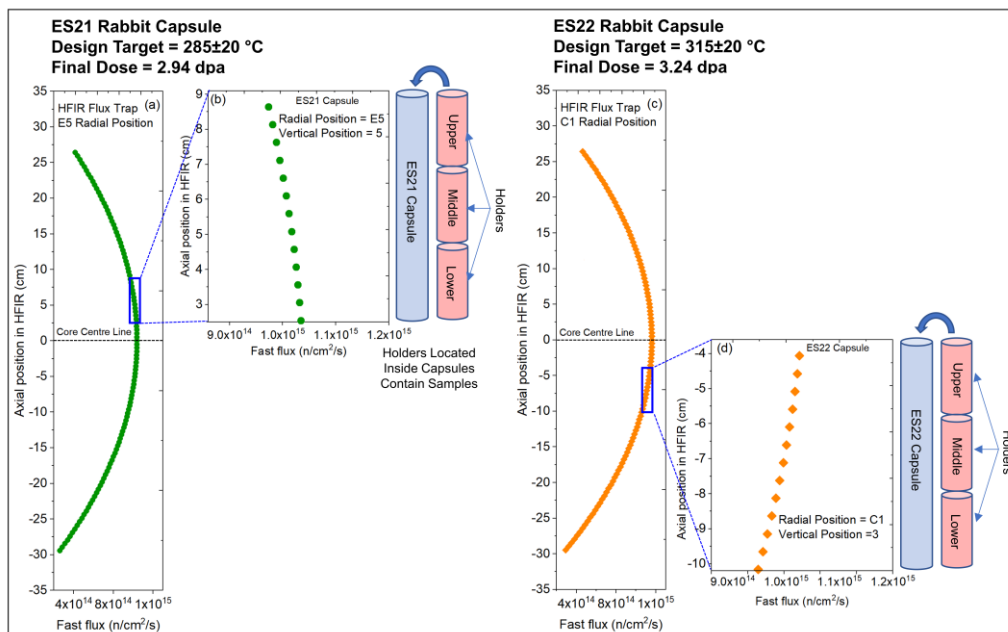


Fig. A1: Average axial fast neutron ($E > 0.1$ MeV) flux profiles for the HFIR rabbit capsule irradiations. (a). Axial flux profile for radial position E5 in the flux trap of HFIR. (b) Axial flux profile for the vertical position #5 in E5 where the first capsule (id = ES21) was located. (c) Axial flux profile for the radial position C1 in the flux trap. (d) Axial flux profile for the vertical position #3 in C1 where the second capsule (id = ES22) was located. From top to bottom of the capsules, the neutron flux varied less than $\sim 7\%$. The capsule/holder schematics shown in (b, d) are roughly to the y-axis scale where the length of one capsule is ~ 6.5 cm. The SS-J3 samples were located inside the holders, implying negligible ($< 2\%$) flux and dose variation from grip to grip. Blue squares represent the capsule & its vertical location. Neutron flux data compiled using Ref. [70].

Appendix B: Temperature distribution across SS-J3 samples

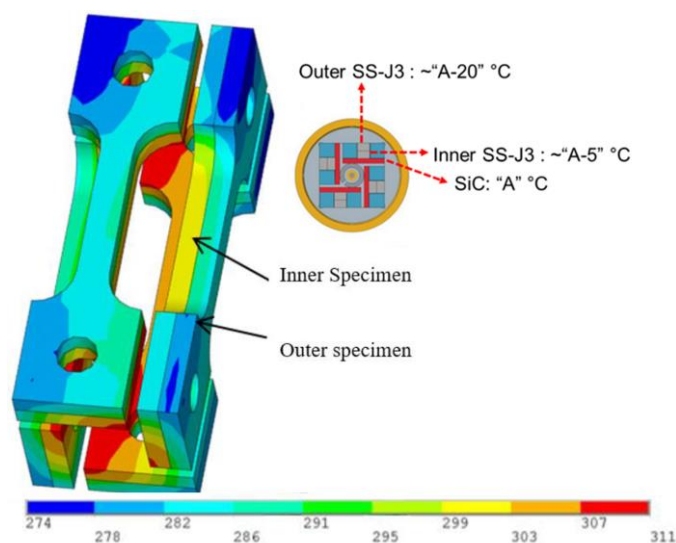


Fig. A2: Specimen temperature analysis using FEM for the tensile samples, adapted from Ref. [71] and the actual specimen temperature estimation methodology by combining SiC thermometry results the FEM results [62]. In this figure, A refers to the temperature value obtained from SiC passive thermometry.

Appendix C: Collection of Vickers hardness data point from grip-to-grip of each SS-J3 sample.

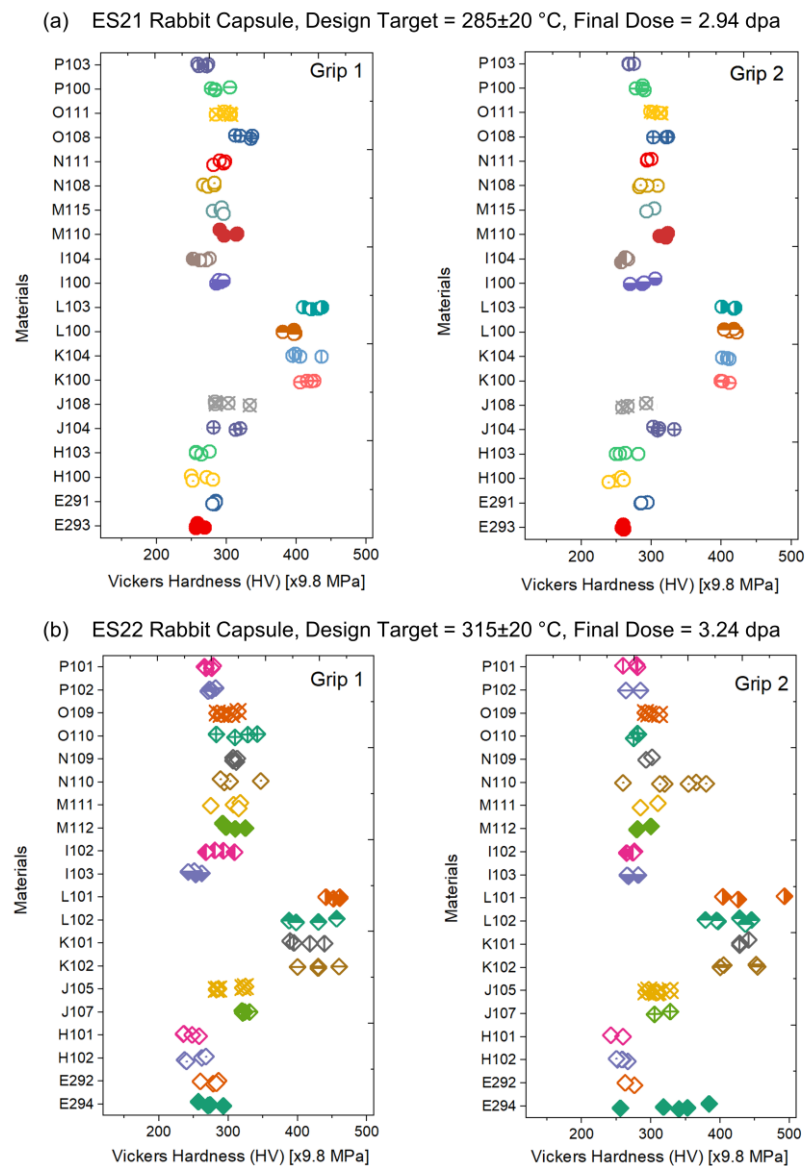


Fig. A3: Value of each Vickers microhardness data point measured on the two grip sections of forty neutron irradiated SS-J3 tensile samples. Individual sample ids of the materials are presented on the y-axis for future traceability using ORNL's hot-cell database. A) ES21 = id of capsule that reached 2.94 dpa at a design target temperature of 285°C. b) ES22 = id of capsule that reached 3.24 dpa at a design target temperature of 315°C. Some samples showed large variance in hardness from one grip to another on the tensile sample - such as N110, E294

etc. These samples were excluded from tensile tests. Grip 1 versus grip 2 were defined arbitrarily for each specimen.

Appendix D: Summary of the tensile data.

Table A1: Unirradiated tensile properties of the ten Eurofer97 steel variants. $T_{test} = RT$ and $300\text{ }^{\circ}C$. σ_{YS} = yield stress, σ_{UTS} = ultimate tensile stress, UE_p = uniform plastic elongation, TE_p = total plastic elongation.

| Steels | Unirradiated | | | | | | | |
|--------|----------------------|-----------------------|--------------------|-------------|-----------------------------------|-----------------------|--------------------|-------------|
| | $T_{test} = RT$ | | | | $T_{test} = 300\text{ }^{\circ}C$ | | | |
| | σ_{YS} MPa | σ_{UTS} MPa | Elongation plastic | | σ_{YS} MPa | σ_{UTS} MPa | Elongation plastic | |
| | | | UE_p % | TE_p % | | | UE_p % | TE_p % |
| H | 402 | 548 | 13.0 | 35.4 | 327 | 426 | 8.0 | 24.0 |
| I | 467 | 603 | 12.0 | 32.3 | 359 | 470 | 8.3 | 23.3 |
| J | 491 | 628 | 9.0 | 29.0 | 423 | 529 | 4.5 | 19.4 |
| K | 802 | 862 | 2.8 | 17.1 | 698 | 769 | 2.0 | 15.0 |
| L | 868 | 960 | 5.0 | 18.0 | 703 | 808 | 3.0 | 15.4 |
| M | 552 | 679 | 9.0 | 24.5 | 418 | 523 | 4.0 | 19.0 |
| N | 513 | 617 | 6.4 | 28.0 | 414 | 477 | 3.0 | 20.0 |
| O | 576 | 682 | 6.1 | 22.6 | 465 | 538 | 3.3 | 14.2 |
| P | 482 | 618 | 12.0 | 31.0 | 388 | 488 | 5.5 | 21.4 |
| E | 474 | 577 | 6.5 | 18.6 | 420 | 516 | 4.0 | 17.0 |

Table A2: Irradiated tensile properties of the ten Eurofer97 steel variants after HFIR neutron irradiation to 2.94 – 3.24 dpa. $T_{irr} = 300\pm 30\text{ }^{\circ}C$. $T_{test} = RT$ and $300\text{ }^{\circ}C$. Symbols have same meaning as in Table A1.

| Steels | Irradiated | | | | | | | |
|--------|-----------------------------------|-----------------------|--------------------|-------------|----------------------|-----------------------|--------------------|-------------|
| | $T_{test} = 300\text{ }^{\circ}C$ | | | | $T_{test} = RT$ | | | |
| | σ_{YS} MPa | σ_{UTS} MPa | Elongation plastic | | σ_{YS} MPa | σ_{UTS} MPa | Elongation plastic | |
| | | | UE_p % | TE_p % | | | UE_p % | TE_p % |
| H | 550 | 571 | 1.1 | 12.3 | 590 | 660 | 3.0 | 16.7 |
| I | 551 | 608 | 2.0 | 13.4 | 668 | 720 | 3.0 | 17.2 |
| J | 584 | 643 | 1.1 | 12.4 | 615 | 731 | 3.8 | 16.7 |
| K | 830 | 896 | 1.0 | 11.0 | 1047 | 1086 | 1.0 | 12.0 |
| L | 937 | 987 | 0.7 | 9.0 | 984 | 1069 | 2.3 | 13.0 |

| | | | | | | | | |
|---|-----|-----|-----|------|-----|-------|-----|------|
| M | 580 | 634 | 1.6 | 12.5 | 767 | 811 | 2.0 | 14.2 |
| N | 644 | 677 | 0.5 | 11.2 | 754 | 789 | 1.6 | 14.7 |
| O | 641 | 683 | 0.7 | 10.0 | 839 | 901.4 | 1.1 | 12.0 |
| P | 514 | 573 | 2.0 | 14.7 | 799 | 837 | 0.5 | 13.2 |
| E | 517 | 578 | 1.6 | 13.1 | 780 | 836 | 1.1 | 13.0 |

References

- [1] G. Federici, W. Biel, M.R. Gilbert, R. Kemp, N. Taylor, R. Wenninger, European DEMO design strategy and consequences for materials, *Nucl. Fusion*. 57 (2017) 092002. <https://doi.org/10.1088/1741-4326/57/9/092002>.
- [2] J.L. Boutard, A. Alamo, R. Lindau, M. Rieth, Fissile core and Tritium-Breeding Blanket: structural materials and their requirements, *Comptes Rendus Phys.* 9 (2008) 287–302. <https://doi.org/10.1016/j.crhy.2007.11.004>.
- [3] D. Stork, R. Heidinger, T. Muroga, S.J. Zinkle, A. Moeslang, M. Porton, J.L. Boutard, S. Gonzalez, A. Ibarra, Towards a programme of testing and qualification for structural and plasma-facing materials in “fusion neutron” environments, *Nucl. Fusion*. 57 (2017) 092013. <https://doi.org/10.1088/1741-4326/aa60af>.
- [4] S.J. Zinkle, L.L. Snead, Designing Radiation Resistance in Materials for Fusion Energy, *Annu. Rev. Mater. Res.* 44 (2014) 241–267. <https://doi.org/10.1146/annurev-matsci-070813-113627>.
- [5] A. Bhattacharya, S.J. Zinkle, Cavity Swelling in Irradiated Materials, in: R. Konings, R.E. Stoller (Eds.), *Compr. Nucl. Mater.*, 2nd ed., Oxford, 2020: pp. 406–455. <https://doi.org/10.1016/b978-0-12-803581-8.11599-1>.
- [6] S.J. Zinkle, J.L. Boutard, D.T. Hoelzer, A. Kimura, R. Lindau, G.R.R. Odette, M. Rieth, L. Tan, H. Tanigawa, Development of next generation tempered and ODS reduced activation ferritic/martensitic steels for fusion energy applications, *Nucl. Fusion*. 57 (2017) 092005. <https://doi.org/10.1088/1741-4326/57/9/092005>.

- [7] G.R. Odette, Recent Progress in Developing and Qualifying Nanostructured Ferritic Alloys for Advanced Fission and Fusion Applications, *JOM*. 66 (2014) 2427–2441. <https://doi.org/10.1007/s11837-014-1207-5>.
- [8] R.L. Klueh, D.R. Harries, High-Chromium Ferritic and Martensitic Steels for Nuclear Applications, ASTM, Bridgeport, 2001. <https://doi.org/10.1520/MONO3-EB>.
- [9] Y.R. Lin, A. Bhattacharya, D. Chen, J.J. Kai, J. Henry, S.J. Zinkle, Temperature-dependent cavity swelling in dual-ion irradiated Fe and Fe-Cr ferritic alloys, *Acta Mater.* 207 (2021) 116660. <https://doi.org/10.1016/j.actamat.2021.116660>.
- [10] B. Raj, M. Vijayalakshmi, Ferritic steels and advanced ferritic-martensitic steels, in: R.J.M. Konings, R.E. Stoller (Eds.), *Compr. Nucl. Mater.*, Elsevier Inc., 2012: pp. 97–121. <https://doi.org/10.1016/B978-0-08-056033-5.00066-5>.
- [11] F. Tavassoli, Eurofer steel, development to full code qualification, *Procedia Eng.* 55 (2013) 300–308. <https://doi.org/10.1016/j.proeng.2013.03.258>.
- [12] B. Van der Schaaf, F. Tavassoli, C. Fazio, E. Rigal, E. Diegele, R. Lindau, G. LeMarois, The development of EUROFER reduced activation steel, *Fusion Eng. Des.* 69 (2003) 197–203. [https://doi.org/10.1016/S0920-3796\(03\)00337-5](https://doi.org/10.1016/S0920-3796(03)00337-5).
- [13] M. Matijasevic, E. Lucon, A. Almazouzi, Behavior of ferritic/martensitic steels after n-irradiation at 200 and 300 °C, *J. Nucl. Mater.* 377 (2008) 101–108. <https://doi.org/10.1016/j.jnucmat.2008.02.063>.
- [14] M. Klimenkov, E. Materna-Morris, A. Möslang, Characterization of radiation induced defects in EUROFER 97 after neutron irradiation, *J. Nucl. Mater.* 417 (2011) 124–126. <https://doi.org/10.1016/j.jnucmat.2010.12.261>.
- [15] X. Chen, L.N. Clowers, T. Graening, A. Bhattacharya, A.A. Campbell, J. Robertson, J.W. Geringer, M.A. Sokolov, Y. Katoh, M. Rieth, Post-irradiation evaluation of eurofer97 fracture toughness using miniature multinotch bend bar specimens, in: *Am.*

- Soc. Mech. Eng. Press. Vessel. Pip. Div. PVP, 2020: pp. 1–8.
<https://doi.org/10.1115/PVP2020-21312>.
- [16] E. Gaganidze, C. Petersen, E. Materna-Morris, C. Dethloff, O.J. Weiß, J. Aktaa, A. Povstyanko, A. Fedoseev, O. Makarov, V. Prokhorov, Mechanical properties and TEM examination of RAFM steels irradiated up to 70 dpa in BOR-60, *J. Nucl. Mater.* 417 (2011) 93–98. <https://doi.org/10.1016/j.jnucmat.2010.12.047>.
- [17] E. Gaganidze, J. Aktaa, J.A. Karlsruher, J. Aktaa, Assessment of neutron irradiation effects on RAFM steels, *Fusion Eng. Des.* 88 (2013) 118–128.
<https://doi.org/10.1016/j.fusengdes.2012.11.020>.
- [18] E. Gaganidze, H.C. Schneider, B. Dafferner, J. Aktaa, Embrittlement behavior of neutron irradiated RAFM steels, *J. Nucl. Mater.* 367-370 A (2007) 81–85.
<https://doi.org/10.1016/j.jnucmat.2007.03.163>.
- [19] L. Boulanger, Y. Serruys, Dislocation loops in Eurofer and a Fe-Cr alloy irradiated by ions at 350 and 550 C at 3 dpa: Effect of dose rate, *J. Nucl. Mater.* 386–388 (2009) 441–444. <https://doi.org/10.1016/j.jnucmat.2008.12.150>.
- [20] B. Kaiser, C. Dethloff, E. Gaganidze, D. Brimbal, M. Payet, P. Trocellier, L. Beck, J. Aktaa, TEM study and modeling of bubble formation in dual-beam He⁺/Fe³⁺ ion irradiated EUROFER97, *J. Nucl. Mater.* 484 (2017) 59–67.
<https://doi.org/10.1016/j.jnucmat.2016.11.014>.
- [21] O.J. Weiss, E. Gaganidze, J. Aktaa, Quantitative characterization of microstructural defects in up to 32 dpa neutron irradiated EUROFER97, *J. Nucl. Mater.* 426 (2012) 52–58. <https://doi.org/10.1016/j.jnucmat.2012.03.027>.
- [22] B. Gómez-Ferrer, C. Dethloff, E. Gaganidze, L. Malerba, C. Hatzoglou, C. Pareige, Nano-hardening features in high-dose neutron irradiated Eurofer97 revealed by atom-probe tomography, *J. Nucl. Mater.* 537 (2020).

- <https://doi.org/10.1016/j.jnucmat.2020.152228>.
- [23] B. Kaiser, E. Gaganidze, C. Dethloff, R. Schwaiger, D. Brimbal, M. Payet, L. Beck, J. Aktaa, Investigation of microstructure defects in EUROFER97 under He⁺/Fe³⁺ dual ion beam irradiation, *Nucl. Mater. Energy*. 15 (2018) 148–153.
<https://doi.org/10.1016/j.nme.2018.04.002>.
- [24] M. Klimenkov, U. Jäntschi, M. Rieth, A. Möslang, Correlation of microstructural and mechanical properties of neutron irradiated EUROFER97 steel, *J. Nucl. Mater.* 538 (2020). <https://doi.org/10.1016/j.jnucmat.2020.152231>.
- [25] O. Tissot, G. Sakr, C. Pareige, J. Henry, Effect of irradiation on nanoprecipitation in EM10 alloy - Comparison with Eurofer97, *J. Nucl. Mater.* 531 (2020) 151995.
<https://doi.org/10.1016/j.jnucmat.2020.151995>.
- [26] S.J. Zinkle, N.M. Ghoniem, Operating temperature windows for fusion reactor structural materials, *Fusion Eng. Des.* 51–52 (2000) 55–71.
[https://doi.org/10.1016/S0920-3796\(00\)00320-3](https://doi.org/10.1016/S0920-3796(00)00320-3).
- [27] N. Hashimoto, R. Kasada, B. Raj, M. Vijayalakshmi, Radiation Effects in Ferritic Steels and Advanced Ferritic-Martensitic Steels, in: *Compr. Nucl. Mater.*, Elsevier, 2020: pp. 226–254. <https://doi.org/10.1016/b978-0-12-803581-8.12051-x>.
- [28] T. Yamamoto, G.R. Odette, H. Kishimoto, J.W. Rensman, P. Miao, On the effects of irradiation and helium on the yield stress changes and hardening and non-hardening embrittlement of ~8Cr tempered martensitic steels: Compilation and analysis of existing data, *J. Nucl. Mater.* 356 (2006) 27–49.
<https://doi.org/10.1016/j.jnucmat.2006.05.041>.
- [29] Y. Dai, G.R. Odette, T. Yamamoto, The effects of helium in irradiated structural alloys, in: R.J.M. Konings (Ed.), *Compr. Nucl. Mater.*, Elsevier Inc., 2012: pp. 141–193. <https://doi.org/10.1016/B978-0-08-056033-5.00006-9>.

- [30] Y. Dai, J. Henry, Z. Tong, X. Averty, J. Malaplate, B. Long, Neutron/proton irradiation and He effects on the microstructure and mechanical properties of ferritic/martensitic steels T91 and EM10, *J. Nucl. Mater.* 415 (2011) 306–310. <https://doi.org/10.1016/J.JNUCMAT.2011.04.029>.
- [31] A. Del Nevo, E. Martelli, P. Agostini, P. Arena, G. Bongiovì, G. Caruso, G. Di Gironimo, P.A. Di Maio, M. Eboli, R. Giammusso, F. Giannetti, A. Giovinazzi, G. Mariano, F. Moro, R. Mozzillo, A. Tassone, D. Rozzia, A. Tarallo, M. Tarantino, M. Utili, R. Villari, WCLL breeding blanket design and integration for DEMO 2015: status and perspectives, *Fusion Eng. Des.* 124 (2017) 682–686. <https://doi.org/10.1016/j.fusengdes.2017.03.020>.
- [32] A.A.F. Tavassoli, J.W. Rensman, M. Schirra, K. Shiba, Materials design data for reduced activation martensitic steel type F82H, *Fusion Eng. Des.* 61–62 (2002) 617–628. [https://doi.org/10.1016/S0920-3796\(02\)00255-7](https://doi.org/10.1016/S0920-3796(02)00255-7).
- [33] A.A.F. Tavassoli, A. Alamo, L. Bedel, L. Forest, J.M. Gentzbittel, J.W. Rensman, E. Diegele, R. Lindau, M. Schirra, R. Schmitt, H.C. Schneider, C. Petersen, A.M. Lancha, P. Fernandez, G. Filacchioni, M.F. Maday, K. Mergia, N. Boukos, Baluc, P. Spätig, E. Alves, E. Lucon, Materials design data for reduced activation martensitic steel type EUROFER, in: *J. Nucl. Mater.*, North-Holland, 2004: pp. 257–262. <https://doi.org/10.1016/j.jnucmat.2004.04.020>.
- [34] E. Gaganidze, H.-C.C. Schneider, B. Dafferner, J. Aktaa, High-dose neutron irradiation embrittlement of RAFM steels, *J. Nucl. Mater.* 355 (2006) 83–88. <https://doi.org/10.1016/j.jnucmat.2006.04.014>.
- [35] K. Shiba, H. Tanigawa, T. Hirose, T. Nakata, Development of the toughness-improved reduced-activation F82H steel for demo reactor, in: *Fusion Sci. Technol.*, American Nuclear Society, 2012: pp. 145–149. <https://doi.org/10.13182/FST12-A14127>.

- [36] H. Tanigawa, E. Gaganidze, T. Hirose, M. Ando, S.J. Zinkle, R. Lindau, E. Diegele, Development of benchmark reduced activation ferritic/martensitic steels for fusion energy applications, *Nucl. Fusion*. 57 (2017) 092004. <https://doi.org/10.1088/1741-4326/57/9/092004>.
- [37] M. Ando, H. Tanigawa, E. Wakai, R.E. Stoller, Effect of two-steps heat treatments on irradiation hardening in F82H irradiated at 573 K, *J. Nucl. Mater.* 386–388 (2009) 315–318. <https://doi.org/10.1016/j.jnucmat.2008.12.123>.
- [38] E. Wakai, M. Ando, T. Sawai, H. Tanigawa, T. Taguchi, R.E. Stoller, T. Yamamoto, Y. Kato, F. Takada, Effect of heat treatments on tensile properties of F82H steel irradiated by neutrons, *J. Nucl. Mater.* 367-370 A (2007) 74–80. <https://doi.org/10.1016/j.jnucmat.2007.03.164>.
- [39] H. Tanigawa, M. Ando, Y. Katoh, T. Hirose, H. Sakasegawa, S. Jitsukawa, A. Kohyama, T. Iwai, Response of reduced activation ferritic steels to high fluence ion-irradiation, *Nucl. Mater.* 297 (2001) 279–284.
- [40] L. Tan, Y. Katoh, F. Tavassoli, J. Henry, M. Rieth, H. Sakasegawa, H. Tanigawa, Q. Huang, Recent status and improvement of reduced-activation ferritic-martensitic steels for high-temperature service, *J. Nucl. Mater.* 479 (2016) 515–523. <https://doi.org/10.1016/j.jnucmat.2016.07.054>.
- [41] E. Lucon, R. Chaouadi, M. Decréton, Mechanical properties of the European reference RAFM steel (EUROFER97) before and after irradiation at 300 °C, *J. Nucl. Mater.* 329–333 (2004) 1078–1082. <https://doi.org/10.1016/j.jnucmat.2004.04.023>.
- [42] E. Lucon, Mechanical properties of the European reference RAFM steel (EUROFER97) before and after irradiation at 300 °C, EFDA Technology Workprogramme 2002 Tritium Breeding and Materials Materials Development - TTMS-001 Deliverable, SCK.CEN-BLG-962, 2003.

- <https://doi.org/10.1016/j.jnucmat.2004.04.023>.
- [43] H. Tanigawa, K. Shiba, A. Möslang, R.E. Stoller, R. Lindau, M.A. Sokolov, G.R. Odette, R.J. Kurtz, S. Jitsukawa, Status and key issues of reduced activation ferritic/martensitic steels as the structural material for a DEMO blanket, *J. Nucl. Mater.* 417 (2011) 9–15. <https://doi.org/10.1016/j.jnucmat.2011.05.023>.
- [44] E. Lucon, W. Vandermeulen, Overview of the tensile properties of EUROFER in the unirradiated and irradiated conditions, *J. Nucl. Mater.* 386–388 (2009) 254–256. <https://doi.org/10.1016/j.jnucmat.2008.12.109>.
- [45] E. Materna-Morris, A. Möslang, R. Rolli, H.C. Schneider, Effect of helium on tensile properties and microstructure in 9%Cr-WVTa-steel after neutron irradiation up to 15 dpa between 250 and 450 °C, *J. Nucl. Mater.* 386–388 (2009) 422–425. <https://doi.org/10.1016/j.jnucmat.2008.12.157>.
- [46] E. Materna-Morris, A. Möslang, H.C. Schneider, Tensile and low cycle fatigue properties of EUROFER97-steel after 16.3 dpa neutron irradiation at 523, 623 and 723 K, *J. Nucl. Mater.* 442 (2013) S62–S66. <https://doi.org/10.1016/j.jnucmat.2013.03.038>.
- [47] L. V. Boccaccini, G. Aiello, J. Aubert, C. Bachmann, T. Barrett, A. Del Nevo, D. Demange, L. Forest, F. Hernandez, P. Norajitra, G. Porempovic, D. Rapisarda, P. Sardain, M. Utili, L. Vala, Objectives and status of EUROfusion DEMO blanket studies, *Fusion Eng. Des.* 109–111 (2016) 1199–1206. <https://doi.org/10.1016/j.fusengdes.2015.12.054>.
- [48] S. Malang, A.R. Raffray, N.B. Morley, An example pathway to a fusion power plant system based on lead-lithium breeder: Comparison of the dual-coolant lead-lithium (DCLL) blanket with the helium-cooled lead-lithium (HCLL) concept as initial step, *Fusion Eng. Des.* 84 (2009) 2145–2157. <https://doi.org/10.1016/j.fusengdes.2009.02.049>.

- [49] J. Hoffmann, M. Rieth, M. Klimenkov, S. Baumgärtner, Improvement of EUROFER's mechanical properties by optimized chemical compositions and thermo-mechanical treatments, *Nucl. Mater. Energy*. 16 (2018) 88–94.
<https://doi.org/10.1016/j.nme.2018.05.028>.
- [50] A. Puype, L. Malerba, N. De Wispelaere, R. Petrov, J. Sietsma, Effect of processing on microstructural features and mechanical properties of a reduced activation ferritic/martensitic EUROFER steel grade, *J. Nucl. Mater.* 494 (2017) 1–9.
<https://doi.org/10.1016/j.jnucmat.2017.07.001>.
- [51] J. Henry, S. Doriot, S. Vincent, C. Caes, C. Toffolon, P. Wident, E. Piozin, J.-C. Brachet, Improvement Of Eurofer 97 High-Temperature Mechanical Properties Using Non-standard Heat Treatments, 17th International Conference on Fusion Reactor Materials, Aachen, (2015).
- [52] A. Di Schino, C. Testani, L. Pilloni, Effect of thermo-mechanical parameters on the mechanical properties of Eurofer97 steel for nuclear applications, *Open Eng.* 8 (2018) 349–353. <https://doi.org/10.1515/eng-2018-0040>.
- [53] L. Pilloni, C. Cristalli, O. Tassa, L. Bozzetto, E. Zanin, N. Bettocchi, Development of innovative materials and thermal treatments for DEMO water cooled blanket, *Nucl. Mater. Energy*. 19 (2019) 79–86. <https://doi.org/10.1016/j.nme.2019.01.026>.
- [54] E. Wakai, M. Ando, S. Matsukawa, T. Taguchi, T. Yamamoto, H. Tomita, F. Takada, Effect of initial heat treatment on DBTT of F82H steel irradiated by neutrons, in: *Fusion Sci. Technol.*, American Nuclear Society, 2005: pp. 856–860.
<https://doi.org/10.13182/FST05-A793>.
- [55] T.S. Byun, D.T. Hoelzer, J.H. Kim, S.A. Maloy, A comparative assessment of the fracture toughness behavior of ferritic-martensitic steels and nanostructured ferritic alloys, *J. Nucl. Mater.* 484 (2017) 157–167.

- <https://doi.org/10.1016/j.jnucmat.2016.12.004>.
- [56] G. Federici, L. Boccaccini, F. Cismondi, M. Gasparotto, Y. Poitevin, I. Ricipito, An overview of the EU breeding blanket design strategy as an integral part of the DEMO design effort, *Fusion Eng. Des.* 141 (2019) 30–42.
<https://doi.org/10.1016/j.fusengdes.2019.01.141>.
- [57] M.R. Gilbert, S.L. Dudarev, S. Zheng, L.W. Packer, J.-C. Sublet, An integrated model for materials in a fusion power plant: transmutation, gas production, and helium embrittlement under neutron irradiation, *Nucl. Fusion.* 52 (2012) 083019.
<https://doi.org/10.1088/0029-5515/52/8/083019>.
- [58] R.L. Klueh, A.T. Nelson, Ferritic/martensitic steels for next-generation reactors, *J. Nucl. Mater.* 371 (2007) 37–52. <https://doi.org/10.1016/j.jnucmat.2007.05.005>.
- [59] R.L. Klueh, N. Hashimoto, P.J. Maziasz, Development of new nano-particle-strengthened martensitic steels, *Scr. Mater.* 53 (2005) 275–280.
<https://doi.org/10.1016/j.scriptamat.2005.04.019>.
- [60] A. Kohyama, K. Hamada, H. Matsui, Specimen size effects on tensile properties of neutron-irradiated steels, *J. Nucl. Mater.* 179–181 (1991) 417–420.
[https://doi.org/10.1016/0022-3115\(91\)90113-L](https://doi.org/10.1016/0022-3115(91)90113-L).
- [61] M. Rieth, E. Simondon, G. Pintsuk, G. Aiello, J. Henry, D. Terentyev, A. Puype, C. Cristalli, L. Pilloni, O. Tassa, M. Klimenkov, H.-C. Schneider, P. Fernandez, T. Gräning, X. Chen, A. Bhattacharya, J. Reed, J.W. Geringer, M. Sokolov, Y. Katoh, L. Snead, Technological aspects in blanket design: Effects of micro-alloying and thermo-mechanical treatments of EUROFER97 type steels after neutron irradiation, *Fusion Eng. Des.* 168 (2021) 112645. <https://doi.org/10.1016/j.fusengdes.2021.112645>.
- [62] A. Bhattacharya, X. Chen, T. Graening, J. Reed, J.W. Geringer, Y. Kato, Post-irradiation examination of Eurofer97 steel variants irradiated to 2.5 dpa, ~300 °C,

- ORNL/SPR-2020/1440, Oak Ridge, TN (United States), 2020.
- [63] A. Bhattacharya, X. Chen, K. Linton, Y. Yamamoto, M. Sokolov, L. Clowers, Y. Katoh, Mechanical properties and microstructure characterization of unirradiated Eurofer-97 steel variants for the EURO fusion project, ORNL/SPR-2018/882 , ORNL Technical Report, 2018. [https://doi.org/https://doi.org/10.2172/1471901](https://doi.org/10.2172/1471901).
- [64] X. Chen, M.A. Sokolov, A. Bhattacharya, L.N. Clowers, T. Graening, Y. Katoh, M. Rieth, Master curve fracture toughness characterization of EuroFer97 steel variants using miniature multi-notch bend bar specimens for fusion applications, in: Am. Soc. Mech. Eng. Press. Vessel. Pip. Div. PVP, 2019. <https://doi.org/10.1115/PVP2019-93797>.
- [65] X. Chen, A. Bhattacharya, M.A. Sokolov, L.N. Clowers, Y. Yamamoto, T. Graening, K.D. Linton, Y. Katoh, M. Rieth, Mechanical properties and microstructure characterization of Eurofer97 steel variants in EUROfusion program, Fusion Eng. Des. 146 (2019) 2227–2232. <https://doi.org/10.1016/j.fusengdes.2019.03.158>.
- [66] A. Bhattacharya, C.M. Parish, J. Henry, Y. Katoh, High throughput crystal structure and composition mapping of crystalline nanoprecipitates in alloys by transmission Kikuchi diffraction and analytical electron microscopy, Ultramicroscopy. 202 (2019) 33–43. <https://doi.org/10.1016/j.ultramic.2019.03.015>.
- [67] L. Pilloni, C. Cristalli, O. Tassa, I. Salvatori, S. Storai, Grain size reduction strategies on Eurofer, Nucl. Mater. Energy. 17 (2018) 129–136. <https://doi.org/10.1016/j.nme.2018.06.023>.
- [68] F. Abe, Precipitate design for creep strengthening of 9% Cr tempered martensitic steel for ultra-supercritical power plants, Sci. Technol. Adv. Mater. 9 (2008) 013002. <https://doi.org/10.1088/1468-6996/9/1/013002>.
- [69] A.G. Le Coq, R.H. Howard, K.D. Linton, K.G. Field, Design and Thermal Analysis

- for Irradiation of Tensile Specimens from Wrought, Powder Metallurgy, and Additive Processed Alloys in the HFIR, ORNL/SPR-2018/959, ORNL Technical Report, 2018. <https://doi.org/10.2172/1474529>.
- [70] T. Daly, J. McDuffee, Experimental and Computational Study of the Flux Spectrum in Materials Irradiation Facilities of the High Flux Isotope Reactor, in: PHYSOR 2012, Adv. React. Phys. Link. Res. Ind. Educ., American Nuclear Society, Knoxville, 2012: pp. 1–14.
- [71] R.H. Howard, K.R. Smith, Development of a Flexible Design for Irradiation of Miniature Tensile and Charpy Test Specimens in the High Flux Isotope Reactor, ORNL/TM-2018/872, 2018.
- [72] A.A. Campbell, W.D. Porter, Y. Katoh, L.L. Snead, Method for analyzing passive silicon carbide thermometry with a continuous dilatometer to determine irradiation temperature, Nucl. Instruments Methods Phys. Res. Sect. B Beam Interact. with Mater. Atoms. 370 (2016) 49–58. <https://doi.org/10.1016/j.nimb.2016.01.005>.
- [73] E. Gaganidze, B. Dafferner, H. Ries, R. Rolli, H.-C. Schneider, J. Aktaa, Irradiation Programme HFR Phase IIb – SPICE Impact testing on up to 16 . 3 dpa irradiated RAFM steels. Final Report for Task TW2-TTMS 001b-D05, 2008.
- [74] K.G. Field, J. McDuffee, J.W. Geringer, C.M. Petrie, Y. Katoh, Evaluation of the continuous dilatometer method of silicon carbide thermometry for passive irradiation temperature determination, Nucl. Instruments Methods Phys. Res. Sect. B Beam Interact. with Mater. Atoms. 445 (2019) 46–56.
- [75] D. Chandler, R.T. Primm, G. Ivan Maldonado, Power distribution analysis for the ornl high flux isotope reactor critical experiment 3, Nucl. Sci. Eng. 164 (2010) 53–68. <https://doi.org/10.13182/NSE09-03>.
- [76] A. Möslang, D. Preininger, Effect of helium implantation on the mechanical properties

- and the microstructure of the martensitic 12% Cr-steel 1.4914, *J. Nucl. Mater.* 155–157 (1988) 1064–1068. [https://doi.org/10.1016/0022-3115\(88\)90468-0](https://doi.org/10.1016/0022-3115(88)90468-0).
- [77] D.S. Gelles, The Consequences of Helium Production and Nickel Additions on Microstructural Development in Isotopically Tailored Ferritic Alloy, in: F.A. Garner, A.S. Kumar (Eds.), *Eff. Radiat. Mater. 18th Int. Symp. ASTM STP 1325*, American Society for Testing and Materials, Philadelphia, 1999: p. 899.
- [78] T. Hirose, M.A. Sokolov, M. Ando, H. Tanigawa, K. Shiba, R.E. Stoller, G.R. Odette, Irradiation response in weldment and HIP joint of reduced activation ferritic/martensitic steel, F82H, *J. Nucl. Mater.* 442 (2013) S557–S561. <https://doi.org/10.1016/j.jnucmat.2013.05.063>.
- [79] J. Henry, S.A. Maloy, Irradiation-resistant ferritic and martensitic steels as core materials for Generation IV nuclear reactors, in: *Struct. Mater. Gener. IV Nucl. React.*, Elsevier Inc., 2017: pp. 329–355. <https://doi.org/10.1016/B978-0-08-100906-2.00009-4>.
- [80] T.S. Byun, K. Farrell, M. Li, Deformation in metals after low-temperature irradiation: Part I - Mapping macroscopic deformation modes on true stress-dose plane, *Acta Mater.* 56 (2008) 1044–1055. <https://doi.org/10.1016/j.actamat.2007.10.061>.
- [81] D.A. McClintock, M.A. Sokolov, D.T. Hoelzer, R.K. Nanstad, Mechanical properties of irradiated ODS-EUROFER and nanocluster strengthened 14YWT, *J. Nucl. Mater.* 392 (2009) 353–359. <https://doi.org/10.1016/j.jnucmat.2009.03.024>.
- [82] G. Aiello, J. Aktaa, F. Cismondi, G. Rampal, J.F. Salavy, F. Tavassoli, Assessment of design limits and criteria requirements for Eurofer structures in TBM components, *J. Nucl. Mater.* 414 (2011) 53–68. <https://doi.org/10.1016/j.jnucmat.2011.05.005>.
- [83] A. Alamo, J.L. Bertin, V.K. Shamardin, P. Wident, Mechanical properties of 9Cr martensitic steels and ODS-FeCr alloys after neutron irradiation at 325 °C up to 42

- dpa, *J. Nucl. Mater.* 367-370 A (2007) 54–59.
<https://doi.org/10.1016/j.jnucmat.2007.03.166>.
- [84] K. Shiba, M. Suzuki, A. Hishinuma, Irradiation response on mechanical properties of neutron irradiated F82H, *J. Nucl. Mater.* 233–237 (1996) 309–312.
[https://doi.org/10.1016/S0022-3115\(96\)00223-1](https://doi.org/10.1016/S0022-3115(96)00223-1).
- [85] J. Vanaja, K. Laha, S. Sam, M. Nandagopal, S. Panneer Selvi, M.D. Mathew, T. Jayakumar, E. Rajendra Kumar, Influence of strain rate and temperature on tensile properties and flow behaviour of a reduced activation ferritic-martensitic steel, *J. Nucl. Mater.* 424 (2012) 116–122. <https://doi.org/10.1016/j.jnucmat.2012.02.020>.
- [86] A.H. Cottrell, M.H. Jaswon, Distribution of solute atoms round a slow dislocation, *Proc. R. Soc. London. Ser. A. Math. Phys. Sci.* 199 (1949) 104–114.
<https://doi.org/10.1098/rspa.1949.0128>.
- [87] T.S. Byun, M.B. Toloczko, T.A. Saleh, S.A. Maloy, Irradiation dose and temperature dependence of fracture toughness in high dose HT9 steel from the fuel duct of FFTF, *J. Nucl. Mater.* 432 (2013) 1–8. <https://doi.org/10.1016/j.jnucmat.2012.07.019>.
- [88] J.H. Baek, T.S. Byun, S.A. Maloy, M.B. Toloczko, Investigation of temperature dependence of fracture toughness in high-dose HT9 steel using small-specimen reuse technique, *J. Nucl. Mater.* 444 (2014) 206–213.
<https://doi.org/10.1016/j.jnucmat.2013.09.029>.
- [89] T. Nozawa, H. Sakasegawa, X. Chen, T. Kato, J.W. Geringer, Y. Katoh, H. Tanigawa, Non-contact strain evaluation for miniature tensile specimens of neutron-irradiated F82H by digital image correlation, *Fusion Eng. Des.* 157 (2020) 111663.
<https://doi.org/10.1016/j.fusengdes.2020.111663>.
- [90] D. De Meis, Structural Materials for DEMO R&D Status, ENEA Report, RT/2015/25 (2015).

- [91] ACFEN, RCC-MRx, Edition 2018, Design and Construction Rules for mechanical components of nuclear installations : high-temperature, research and fusion, reactors, Association Francaise pour les regles de Conception et de Construction des Materiels des Chaudières Electro-nucleaires, 2018.
- [92] P. Bridgman, Studies in large plastic flow and fracture, Mc-Graw Hill Book Company, London, 1952. [https://doi.org/10.1016/0016-0032\(52\)90513-9](https://doi.org/10.1016/0016-0032(52)90513-9).
- [93] E. Wakai, T. Taguchi, T. Yamamoto, F. Takada, Effect of tempering temperature and time on tensile properties of F82H irradiated by neutrons, *J. Nucl. Mater.* 329–333 (2004) 1133–1136. <https://doi.org/10.1016/j.jnucmat.2004.04.037>.
- [94] C. Cabet, F. Dalle, E. Gaganidze, J. Henry, H. Tanigawa, Ferritic-martensitic steels for fission and fusion applications, *J. Nucl. Mater.* 523 (2019) 510–537. <https://doi.org/10.1016/j.jnucmat.2019.05.058>.
- [95] K. Farrell, T.S. Byun, Tensile properties of ferritic/martensitic steels irradiated in HFIR, and comparison with spallation irradiation data, *J. Nucl. Mater.* 318 (2003) 274–282. [https://doi.org/10.1016/S0022-3115\(03\)00102-8](https://doi.org/10.1016/S0022-3115(03)00102-8).
- [96] G. Yeli, V.C.I. Strutt, M.A. Auger, P.A.J. Bagot, M.P. Moody, Characterisation of nano-scale precipitates in BOR60 irradiated T91 steel using atom probe tomography, *J. Nucl. Mater.* 543 (2021) 152466. <https://doi.org/10.1016/j.jnucmat.2020.152466>.
- [97] J.T. Busby, M.C. Hash, G.S. Was, The relationship between hardness and yield stress in irradiated austenitic and ferritic steels, *J. Nucl. Mater.* 336 (2005) 267–278. <https://doi.org/10.1016/j.jnucmat.2004.09.024>.
- [98] M. Umemoto, Z.G. Liu, K. Tsuchiya, S. Sugimoto, M.M.A. Bepari, Relationship between hardness and tensile properties in various single structured steels, *Mater. Sci. Technol.* 17 (2001) 505–511. <https://doi.org/10.1179/026708301101510339>.
- [99] Y. Yano, T. Tanno, Y. Sekio, H. Oka, S. Ohtsuka, T. Uwaba, T. Kaito, Tensile

- properties and hardness of two types of 11Cr-ferritic/martensitic steel after aging up to 45,000 h, *Nucl. Mater. Energy*. 9 (2016) 324–330.
<https://doi.org/10.1016/j.nme.2016.08.007>.
- [100] G.E. Dieter, *Mechanical Metallurgy*, 3rd ed., McGraw Hill, 1986.
- [101] T.S. Byun, K. Farrell, Plastic instability in polycrystalline metals after low temperature irradiation, *Acta Mater.* 52 (2004) 1597–1608.
<https://doi.org/10.1016/j.actamat.2003.12.023>.
- [102] B. van der Schaaf, C. Petersen, Y. De Carlan, J.W. Rensman, E. Gaganidze, X. Averty, High dose, up to 80 dpa, mechanical properties of Eurofer 97, *J. Nucl. Mater.* 386–388 (2009) 236–240. <https://doi.org/10.1016/j.jnucmat.2008.12.329>.
- [103] S.J. Zinkle, J.P. Robertson, R. Klueh, Thermophysical and mechanical properties of Fe-(8-9%)Cr reduced activation steels, *Fusion Materials Semiann. Prog. Report for period ending June 30 1998*, DOE/ER-0313/24, Oak Ridge, 1998.
- [104] A. Alamo, M. Horsten, X. Averty, E.I. Materna-Morris, M. Rieth, J.C. Brachet, Mechanical behavior of reduced-activation and conventional martensitic steels after neutron irradiation in the range 250-450 °C, *J. Nucl. Mater.* 283–287 (2000) 353–357.
[https://doi.org/10.1016/S0022-3115\(00\)00076-3](https://doi.org/10.1016/S0022-3115(00)00076-3).